NASA Contractor Report 182003
ICASE Report No. 90–19

AD–A227 205

ICASE

SURFACE — COOLING EFFECTS ON COMPRESSIBLE BOUNDARY — LAYER INSTABILITY

S. O. Seddougui
R. I. Bowles
F. T. Smith

DTIC
S ELECTE
OCT 0 3 1990
E
D

NASA

National Aeronautics and
Space Administration

Langley Research Center
Hampton, Virginia 23665-5225

90

90 04 02 140

Surface - Cooling Effects on Compressible
Boundary - Layer Instability

S. O. Seddougui[1]

Institute for Computer Applications in Science and Engineering

NASA Langley Research Center

Hampton, VA 23665

R. I. Bowles and F. T. Smith

University College London

Gower Street

London WC1E 6BT

Abstract

The influence of surface cooling on compressible boundary-layer instability is discussed theoretically for both viscous and inviscid modes, at high Reynolds numbers. The cooling enhances the surface heat transfer and shear stress, creating a high-heat-transfer sublayer. This has the effect of distorting and accentuating the viscous Tollmien-Schlichting modes to such an extent that their spatial growth rates become comparable with, and can even *exceed*, the growth rates of inviscid modes, including those found previously. This is for moderate cooling, and it applies at any Mach number. In addition, the moderate cooling destabilizes otherwise stable viscous or inviscid modes, in particular triggering outward-traveling waves at the edge of the boundary layer in the supersonic regime. Severe cooling is also discussed as it brings compressible dynamics directly into play within the viscous sublayer. All the new cooled modes found involve the heat-transfer sublayer quite actively, and they are often multi-structured in form and may be distinct from those observed in previous computational and experimental investigations. The corresponding nonlinear processes are also pointed out with regard to transition in the cooled compressible boundary layer. Finally, comparisons with Lysenko and Maslov's (1984) experiments on surface cooling are presented.

---

i

1. INTRODUCTION

Surface cooling is fairly often applied on supersonic-hypersonic flight vehicles, and in some cases it is essential for the preservation of the vehicle itself, especially at higher Mach numbers. The effects of such cooling on the instability and transition properties of the local compressible boundary-layer flow are then of much concern. Given the practical importance, it is perhaps surprising that there are not more experimental, theoretical and computational studies of surface-cooling effects on instability and transition; see the experiments of Van Driest and McCauley (1957), Wisniewski and Jack (1960), Richards and Stollery (1966), Stetson and Rushton (1967), Van Driest and Blumer (1968), Kendall (1975), Demetriades (1978), Lysenko and Maslov (1981,1984), and the theoretical suggestions and computations of Lees and Lin (see Lin 1955), Reshotko (1963), Mack (1969,1975,1984,1986), Maslov (1974), Gapanov and Maslov (1980), Malik (1987). The flow phenomena produced can be complex, and the findings and suggestions from the works above are a little mixed, but Lysenko and Maslov (1984) seem to provide a reasonable overall summary, namely that the so-called first modes tend to be stabilized by surface cooling whereas the second modes are destabilized to a limited extent. Also, islands of first-mode instability have been predicted by parallel-flow theory at the lower Reynolds numbers, although these suggestions are questionable due to the nonparallel-flow effects present then: see also later.

The present theoretical investigation, in comparison, suggests that the effects of surface cooling can be much more pronounced and "dangerous." In particular it is found that the cooling, even if only moderate, so distorts the viscous-inviscid Tollmien-Schlichting (TS) modes [first modes] that their spatial growth rates can become comparable with or larger than those of the inviscid modes [second and higher modes] described above, at high Reynolds numbers. This reversal of the usual ordering of the instabilities arises because of the enhanced heat transfers and shear stresses produced in the basic boundary-layer flow at the surface by the presence of cooling, which results in a sublayer of high heat transfer emerging on the surface. The increased surface shear stresses cause the typical viscous-inviscid TS wavelength to be decreased and the flow structure associated with the TS wave is soon altered, as the surface is cooled, bringing about the rise in growth rates, as well as rendering previously stable modes unstable.

The present predictions appear to agree broadly with Lysenko and Maslov's (1984) summary finding above, and with their experiments for supersonic boundary layers (see also the comparisons in §6 below), in that the wavenumbers and frequencies associated with the boundary-layer's first-mode instability increase with surface cooling, at a given Reynolds number. There is however some possible disagreement as well (which may be a matter of interpretation) in the sense that the theoretical growth rates increase also, as described in

1

the previous paragraph. Thus the prediction here is that, with cooling, instability may be delayed but when it occurs it is likely to be more violent than in the non-cooled, e.g. insulated, case. This is mainly for the viscous-inviscid first modes, but similar findings emerge for the inviscid second modes also as discussed later.

"Moderate cooling" of the surface, and its influence on the compressible viscous modes, is dealt with in §§2 and 3 below, based on the theory in Smith (1987). The new flow structure produced is examined first, followed by its instability properties. The flow structure is of the compressible Rayleigh inviscid kind across the majority of the boundary layer, but in a quasi-steady form, which admits pressure-displacement interaction with the viscous sublayer response. Unlike the non-cooled TS instability modes, which in supersonic flow must be directed outside the wave-Mach cone, i.e. be effectively subsonic, the present surface-cooled ones can be unstable for any obliqueness angle, including the two-dimensional (2D) case. This and other factors of the link between the cooled and the non-cooled TS modes are also explored in §3, along with the influence of cooling the surface beyond the moderate stage. There the spatial growth rates become still more accentuated, for any Mach number, as the viscous-inviscid disturbance is concentrated relatively near the surface, and flow-structural change re-occurs. We devote a separate section, §4, to the resulting stage of "severe cooling", to emphasize its novel nature. This concerns principally the intrusion of compressibility effects into the dynamics of the thin viscous sublayer. Although the work overall is mostly on viscous modes, pure inviscid modes are addressed in §5 as a result of the behavior found earlier in the moderate-cooling regime. Once again, cooled-surface modes which appear to be distinct from those found in earlier studies are implied, for any Mach number M_∞, with the heat-transfer sublayer playing an active part throughout. The new inviscid modes, like the viscous ones of §§2-4, all have relatively small phase speeds, and they include some which radiate, i.e. provoke outward-traveling waves at the edge of the boundary layer.

Nondimensional variables are used such that the freestream velocity is $(u, v, w) = (1, 0, 0)$, in cartesian coordinates (x, y, z) where the airfoil chord is unity. The nondimensional pressure, density, temperature and viscosity are written p, ρ, T, μ in turn, equal to $p_\infty, 1, 1, 1$ in the freestream, where $p_\infty = 1/(\gamma M_\infty^2)$, and t denotes the usual convectively scaled time. The basic boundary layer then has $O(Re^{-1/2})$ characteristic thickness where Re is the global Reynolds number produced above and the boundary-layer properties are defined by the profiles $(u, T, \rho) = (U_0, T_0, \rho_0)(\bar{y})$, with $y = Re^{-1/2}\bar{y}$, at the local station $x = x_0, z = z_0$ under consideration. In §§2-4 nonlinear viscous-inviscid interactions are considered first since the understanding of flow transition is the ultimate theoretical goal, although linear solution properties are then treated, as a first study, since this type of approach for surface cooling appears to be a fresh one. The corresponding nonlinear inviscid versions in §5 can likewise

2

be set up. Further discussion is presented in §6, along with some comparisons with the experiments of Lysenko and Maslov (1984) and related comments.

2. THE MODERATE-COOLING REGIME

For order-one values of the temperature ratio $T_w^*/T_\infty^* (\equiv T_w)$ the compressible three-dimensional TS modes are controlled by the triple-deck structure as described by Smith (1987), as long as the other parameters involved are not too extreme. That structure provides the springboard for the present theory on surface cooling and so its underlying form is noted here. The expressions for the flow solution in the three decks are:

$$upper\ deck,\quad y = Re^{-3/8}K_1 m^{-1/2}y_1\ \ and$$
$$[u, v, w, p] = [1, 0, 0, p_\infty] + Re^{-1/4}C^{1/4}\lambda^{1/2}m^{-1/4}[\overline{u}^{(2)}, m^{1/2}\overline{v}^{(2)}, \overline{w}^{(2)}, \overline{p}^{(2)}];\ \Big\} \quad (2.1a)$$

$$main\ deck,\ y = Re^{-1/2}\overline{y}\ \ and$$
$$[u, v, w, p] = [U_0, 0, 0, p_\infty] + O[Re^{-1/8}, Re^{-1/4}, Re^{-1/4}, Re^{-1/4}];\ \Big\} \quad (2.1b)$$

$$lower\ deck,\ y = Re^{-5/8}m^{-1/8}C^{5/8}T_w^{3/2}\lambda^{-3/4}Y^*\ \ and$$
$$[u, v, w, p] = [Re^{-1/8}C^{1/8}T_w^{1/2}\lambda^{1/4}m^{-1/8}U^*, Re^{-3/8}C^{3/8}T_w^{1/2}\lambda^{3/4}m^{1/8}V^*,$$
$$Re^{-1/8}c^{1/8}T_w^{1/2}\lambda^{1/4}m^{-1/8}W^*, Re^{-1/4}C^{1/4}\lambda^{1/2}m^{-1/4}P^*];\ \Big\} \quad (2.1c)$$

throughout, the streamwise and spanwise length scales and the time scale are given by

$$(x - x_0, z - z_0) = Re^{-3/8}K_1(X^*, Z^*), \quad t = Re^{-1/4}m^{-1/4}T_w C^{1/4}\lambda^{-3/2}t^*. \quad (2.1d)$$

Here $m \equiv |M_\infty^2 - 1|$, and P and $-A$ are the unknown pressure and displacement variations (independent of $\overline{y}, Y^*$), C is the Chapman constant, $\lambda(x_0, z_0)$ is the $O(1)$ skin-friction coefficient of the incident compressible boundary layer and (x_0, z_0) is the local position under consideration, while $K_1 \equiv C^{3/8}T_w^{3/2}\lambda^{-5/4}m^{-3/8}$. Similar expansions hold for the temperature T, the density ρ and the viscosity μ. As a result the overall nonlinear three-dimensional TS behavior here is governed by the lower-deck equations and boundary conditions,

$$U_{X^*}^* + V_{Y^*}^* + W_{Z^*}^* = 0, \quad (2.2a)$$

$$U_{t^*}^* + U^*U_{X^*}^* + V^*U_{Y^*}^* + W^*U_{Z^*}^* = -P_{X^*}^*(X^*, Z^*, t^*) + U_{Y^*Y^*}^*, \quad (2.2b)$$

$$W_{t^*}^* + U^*W_{X^*}^* + V^*W_{Y^*}^* + W^*W_{Z^*}^* = -P_{Z^*}^*(X^*, Z^*, t^*) + W_{Y^*Y^*}^*, \quad (2.2c)$$

$$U^* = V^* = W^* = 0\ at\ Y^* = 0, \quad (2.2d)$$

$$U^* \sim Y^* + A^*(X^*, Z^*, t^*), \quad W^* \to 0,\ as\ Y^* \to \infty, \quad (2.2e)$$

3

coupled through pressure-displacement interaction with the upper-deck linearized potential flow problem (for supersonic and subsonic flow respectively)

$$[(M_\infty^2 - 1)(\partial_{X^*}^2 \mp \partial_{y_u}^2) - \partial_{Z^*}^2]\bar{p}^{(2)} = 0, \tag{2.2f}$$

where

$$\bar{p}^{(2)} \to 0 \text{ as } y_u \to \infty; \quad \bar{p}^{(2)} \to \bar{P}^*, \quad \bar{p}_{y_u}^{(2)} \to A_{X^* X^*}^* \text{ as } y_u \to 0+. \tag{2.2g}$$

Suitable constraints at large $|X^*|, |Z^*|$, are also assumed, and imposed forcing can be incorporated in either or both of the parts (2.2a-e), (2.2f,g). Various nonlinear features of the unsteady viscous-inviscid system (2.2) for nonlinear TS evolution are addressed by Smith & Walton (1989), Smith (1988, 1989) among others, while the linearized version corresponding to relatively small compressible TS waves is studied by Smith (1987). Here we follow the same procedure of setting up the nonlinear stage first and linearizing afterwards, in dealing with surface-cooling effects.

The main impact of surface cooling, i.e. small T_w, is felt partly through the T_w factors themselves in the scales above and partly through the alterations in the mean-flow profiles U_0, T_0 near the surface, specifically in the *large heat transfer and skin friction* produced there. This can be seen in two ways. One is by means of the Howarth-Dorodnitsyn transformation, $y' = \int_0 T_0^{-1} d\bar{y}$, since U_0, T_0 are regular in terms of the transformed variable y'. So if T_w is reduced then initially $T_0 \propto y'$ at small y' with an $O(1)$ constant of proportionality. Hence the transformation implies that $\bar{y} \propto \int_0 T_0 dy'$ is quadratic in y', and therefore the temperature profile T_0 is tending to zero like the *square-root* of the normal distance $\bar{y}$. The same applies to the velocity U_0. That implies large temperature and velocity gradients developing near the surface. The precise size of these is determined by a sublayer produced where $\bar{y}$ is $O(T_w^2)$, or $y' \sim T_w$, and the low surface temperature becomes comparable with the linearly decreasing (in terms of y') contribution above, so that $T_0 \approx T_w + y'$ times $O(1)$, *i.e.* $T_w + O(1)$ times $[\bar{y} + O(1)]^{1/2}$. It follows that the surface heat transfer, $\partial T_0/\partial \bar{y}$ at $\bar{y} = 0$, is $O(T_w^{-1})$. Likewise, the surface shear stress is $O(T_w^{-1})$. The alternative is to consider the basic-flow momentum and heat-flux equations, which are dominated by their viscous contributions near the surface at small $\bar{y}$, i.e. by $\partial(\mu_0 \partial U_0/\partial \bar{y})/\partial \bar{y} = 0$ and $\partial(\mu_0 \partial T_0/\partial \bar{y})/\partial \bar{y} = 0$ respectively. Since $\mu_0 \propto T_0$ for a Chapman fluid (see also later) the second balance above integrates to give $T_0 \partial T_0/\partial \bar{y}$ uniform in $\bar{y}$ and hence T_0^2 is linear in $\bar{y}$; so again the almost square-root response in the temperature T_0 and the large $O(T_w^{-1})$ heat transfer $\partial T_0/\partial \bar{y}$ are implied at small $\bar{y}$ and T_w. Similar results for U_0 stem from the momentum balance above. The effect of surface cooling, then, is to induce a new sublayer in which, for certain $O(1)$ constants c_1, c_2,

$$\bar{y} = T_w^2 \hat{y}, \quad T_0 = T_w(1 + 2c_1\hat{y})^{1/2}, \quad U_0 = T_w\frac{c_2}{c_1}\{(1 + 2c_1\hat{y})^{1/2} - 1\}, \tag{2.3a}$$

and in consequence the scaled heat transfer and skin friction

$$(\partial T_0/\partial \bar{y})_{\bar{y}=0} \sim T_w^{-1}c_1, \quad \lambda \equiv (\partial U_0/\partial \bar{y})_{\bar{y}=0} \sim T_w^{-1}c_2, \qquad (2.3b)$$

are increased substantially.

The implications for the TS waves follow directly from the increase in λ in (2.3b) and the decrease in T_w. Thus the TS length scales of (2.1a,c,d) all shrink now, as might be expected physically, and in particular the streamwise length and the maximum normal distance both decrease like $T_w^{3/2}$. Similar deformations occur in the typical lower-deck thickness and in all the velocity and pressure scales, for instance, and eventually a new flow structure must come into play as T_w continues to drop. Various options present themselves but the first distinct new structure is found to arise when T_w is decreased to the order $Re^{-1/12}$, at which stage the upper-deck extent becomes coincident with the main boundary layer's, as does the streamwise length scale. So novel elliptic effects must then enter the boundary-layer dynamics.

In the new stage of "moderate cooling", therefore, we have

$$T_w = Re^{-1/12}\tilde{T}_w, \qquad (2.4)$$

say, with $\tilde{T}_w$ typically of order unity, and a three-tier structure comes into operation. See Figure 1. The scales and balances involved are suggested by the ones mentioned earlier but combined with (2.4). Across most of the boundary layer, the main tier where $\bar{y}$ is $O(1)$ is given by

$$[u, v, w, p, \rho, T] = [U_0, 0, 0, p_\infty, \rho_0, T_0] + Re^{-1/4}\tilde{\rho}\tilde{\lambda}^2 c_3^2[\bar{u}, \bar{v}, \bar{w}, \bar{p}, \bar{\rho}, \overline{T}] + \cdots \qquad (2.5)$$

with $c_3 \equiv (C/\tilde{\lambda}\tilde{\rho}^2)^{1/3}$, while in the buffer tier where $y = Re^{-2/3}\tilde{y}$

$$[u, v, w, p, \rho, T] = [Re^{-1/12}\tilde{u} + Re^{-1/6}c_3\hat{A}\tilde{u}', -Re^{-1/3}c_3\hat{A}_X\tilde{u}, Re^{-1/4}\tilde{\lambda}^2 c_3^2 D/\tilde{u},$$

$$p_\infty + Re^{-1/4}\tilde{\rho}\tilde{\lambda}^2 c_3^2 P, Re^{1/12}\tilde{\rho}, Re^{-1/12}\tilde{T}_w], \qquad (2.6)$$

to leading order, with $D_X = -P_Z$, and in the lower tier $y = Re^{-3/4}c_3 Y$ with

$$[u, v, w, p, \rho, T] = [Re^{-1/6}\tilde{\lambda}c_3 U, Re^{-5/12}\tilde{\lambda}c_3^2 V, Re^{-1/6}\tilde{\lambda}c_3 W,$$

$$p_\infty + Re^{-1/4}\tilde{\rho}\tilde{\lambda}^2 c_3^2 P, Re^{1/12}\tilde{\rho}, Re^{-1/12}\tilde{T}_w]. \qquad (2.7)$$

Here the extra factors $C, \tilde{\lambda}(\equiv c_2/\tilde{T}_w), \tilde{\rho}(\equiv \tilde{T}_w^{-1})$ present are all $O(1)$ and are included to produce a normalized equation set below, taking account of the scaled surface density, viscosity

and shear values which would otherwise appear in the lower-tier system for example. The streamwise and spanwise length and the time scales now are defined by

$$(x - x_0, z - z_0) = Re^{-1/2}(X, Z), \quad t = \frac{Re^{-1/3}\hat{t}}{\lambda c_3}. \tag{2.8}$$

Hence the main-tier properties are controlled by the linearized quasi-steady inviscid balances

$$\rho_0 \bar{u}_X + \bar{\rho}_X U_0 + \rho_0 \bar{v}_{\bar{y}} + \rho_{0_{\bar{y}}} \bar{v} + \rho_0 \bar{w}_Z = 0, \tag{2.9a}$$

$$U_0 \bar{u}_X + \bar{v} U_{0_{\bar{y}}} = -\bar{p}_X / \rho_0, \tag{2.9b}$$

$$U_0 (\bar{v}_X, \bar{w}_X) = -(\bar{p}_{\bar{y}}, \bar{p}_Z)/\rho_0, \tag{2.9c}$$

$$U_0 (\rho_0 \bar{p}_X - \gamma p_\infty \bar{\rho}_X) = \gamma p_\infty \rho_{0_{\bar{y}}} \bar{v}, \tag{2.9d}$$

leading to the compressible pressure equation

$$\bar{p}_{\bar{y}\bar{y}} + \bar{p}_{ZZ} + (1 - M_0^2)\bar{p}_{XX} = 2M_{0_{\bar{y}}}\bar{p}_{\bar{y}}/M_0, \tag{2.10a}$$

with effectively zero phase speed. Here $M_0 \equiv U_0 M_\infty / T_0^{1/2}$. The constraints on $\bar{p}$ are

$$\bar{p} \to 0 \text{ [or outgoing waves] as } \bar{y} \to \infty, \tag{2.10b}$$

$$\bar{p} \sim P + \frac{2}{3}\tau A_{XX}\bar{y}^{3/2} \text{ as } \bar{y} \to 0+, \tag{2.10c}$$

together with appropriate boundedness conditions far upstream and downstream (see below), where (2.10b) reflects the match with the oncoming undisturbed free-stream motion and (2.10c) is necessary for merging with the buffer tier. The 3/2-dependence in (2.10c) comes from analysis of (2.10a), given that the basic-flow profiles U_0, T_0 exhibit the square-root dependence

$$U_0 \sim c_2 (2/c_1)^{1/2}\bar{y}^{1/2}, \quad T_0 \sim (2c_1)^{1/2}\bar{y}^{1/2}, \text{ as } \bar{y} \to 0+, \tag{2.11}$$

consistent with (2.3). The $O(1)$ parameter τ introduced in (2.10c) is defined by

$$\tau = \frac{c_2^{1/3} 2^{1/2} \tilde{T}_w^2}{c_1^{3/2} C^{1/3}}, \tag{2.12a}$$

for consistency with the buffer tier below. Again, the associated velocity perturbations respond in the form

$$(\bar{u}, \bar{v}, \bar{w}) \sim (\bar{y}^{-1/2}, \bar{y}^{1/2}, O(1)), \tag{2.12b}$$

at small $\bar{y}$, agreeing both with (2.10c) and (2.6). The buffer tier of (2.6) is also governed by predominantly inviscid linear dynamics but it accommodates the basic inner-layer behavior (2.3a), thereby smoothing out the 3/2-dependence, since the velocity profile

$$\tilde{u}(\tilde{y}) = \frac{c_2}{c_1}[(\tilde{T}_w^2 + 2c_1\tilde{y})^{1/2} - \tilde{T}_w], \tag{2.13}$$

is regular. The final, lower, viscous tier of (2.7) then yields the three-dimensional unsteady nonlinear boundary-layer equations,

$$U_X + V_Y + W_Z = 0, \qquad (2.14a)$$

$$U_{\hat{t}} + UU_X + VU_Y + WU_Z = -P_X(X, Z, \hat{t}) + U_{YY}, \qquad (2.14b)$$

$$W_{\hat{t}} + UW_X + VW_Y + WW_Z = -P_Z(X, Z, \hat{t}) + W_{YY}, \qquad (2.14c)$$

subject to the conditions

$$U = V = W = 0 \text{ at } Y = 0, \qquad (2.14d)$$

$$U \sim Y + A(X, Z, \hat{t}), \quad W \to 0, \text{ as } Y \to \infty, \qquad (2.14e)$$

for no slip at the surface and to match with the buffer tier's response in turn.

The nonlinear system describing moderate cooling is therefore given by the viscous-inviscid interaction of (2.10a-c) combined with (2.14a-e). A match may be verified with the earlier structure of (2.1) at large τ, corresponding to large $\tilde{T}_w$, and certain extra aspects of this are examined in the next section. Of most concern here are the properties of the new cooled-surface TS system at $O(1)$ values of τ and the effects of the inviscid but rotational elliptic part (2.10) of the interaction, which represents the major new feature present in the moderate-cooling regime. Further, small-disturbance properties can be of much interest, for practical and other reasons including the fact that the length scales and hence the spatial growth rates expected are now comparable with those of pure inviscid modes, and so we address here the linearized instability version in which $(U, V, W, P, A, \bar{p})$ are taken to be small perturbations of the basic undisturbed state $(Y, 0, 0, 0, 0, 0)$. This has the effect of keeping (2.10a-c) intact but with the lower-tier response becoming linearized. In consequence cool-surface TS waves $\propto \exp(i(\alpha X + \beta Z - \Omega \hat{t}))$ are possible with wavenumbers α, β and frequency Ω, in which case we are left with solving the quasi-steady compressible Rayleigh equation

$$\bar{p}'' - \frac{2M_0'}{M_0}\bar{p}' - [\alpha^2(1 - M_0^2) + \beta^2]\bar{p} = 0, \qquad (2.15a)$$

subject to

$$\bar{p} \to 0 \text{ [or outgoing waves] as } \bar{y} \to \infty, \qquad (2.15b)$$

$$\bar{p} \sim P - \frac{2}{3}\tau\alpha^2 A\bar{y}^{3/2} \text{ as } \bar{y} \to 0+, \qquad (2.15c)$$

and

$$\frac{P}{A} = \frac{(i\alpha)^{-1/3}}{(1 + \beta^2/\alpha^2)} \frac{Ai'(\xi_0)}{\kappa(\xi_0)}, \quad \left(\xi_0 \equiv -i^{1/3}\Omega/\alpha^{2/3}, \; \kappa \equiv \int_{\xi_0}^{\infty} Ai(q)dq\right). \qquad (2.15d)$$

In (2.15a) the prime denotes a $\bar{y}$ - derivative, while (2.15d) stems from the viscous linear lower-tier solution in terms of the Airy function Ai. The properties of the moderate - cooling system (2.15) are investigated in the next section.

7

3. INSTABILITY PROPERTIES FOR MODERATE COOLING

Solutions of the moderate - cooling problem (2.15) were obtained (a) by computation, (b) analytically for small τ, (c) analytically for large τ, connected with relatively high frequencies, and these are described in turn below. In practice, some of the features found in (b), (c) were used to guide the computations in (a), and vice-versa.

3(a). Computational Study

For moderate values of the Mach number we chose the mean-flow profiles U_0 and T_0 to have the following representative forms:

$$U_0 = 1 - e^{-\bar{y}^{1/2}}, \tag{3.1a}$$

$$T_0 = 1 - e^{-\bar{y}^{1/2}}, \tag{3.1b}$$

i.e. they have the required square - root dependencies as $\bar{y} \to 0+$; the decay as $\bar{y} \to \infty$ is of relatively little consequence, we note. Then $M_0 = U_0 M_\infty / T_0^{1/2} = M_\infty (1 - e^{-\bar{y}^{1/2}})^{1/2}$, and the system (2.15) becomes

$$\bar{p}'' - \frac{1}{2}\bar{y}^{-1/2}\frac{e^{-\bar{y}^{1/2}}}{1 - e^{-\bar{y}^{1/2}}}\bar{p}' - (\alpha^2(1 - M_\infty^2(1 - e^{-\bar{y}^{1/2}})) + \beta^2)\bar{p} = 0, \tag{3.2a}$$

with the boundary conditions

$$\bar{p} \to 0 \ (\text{or outgoing waves}) \text{ as } \bar{y} \to \infty, \tag{3.2b}$$

$$\bar{p} \sim P - \frac{2}{3}\tau\alpha^2 A\bar{y}^{3/2} \text{ as } \bar{y} \ 0+, \tag{3.2c}$$

and

$$\frac{P}{A} = \frac{(i\alpha)^{-1/3}}{(1 + \beta^2/\alpha^2)}\frac{Ai'(\xi_0)}{\kappa(\xi_0)}, \tag{3.2d}$$

where ξ_0 and κ are defined by (2.15d). For $\bar{y} \ll 1$ we may obtain two independent solutions of (3.2a), with multiplicative constants a_1, a_2,

$$\bar{p} = a_1\{1 + (\beta^2 + \alpha^2)\bar{y}^2 - \frac{1}{5}(\beta^2 + \alpha^2(1 + 2M_\infty^2))\bar{y}^{5/2} + (\frac{5}{108}(\beta^2 + \alpha^2) + \frac{\alpha^2 M_\infty^2}{6})\bar{y}^3 + \cdots\}$$

$$+a_2\{\bar{y}^{3/2} - \frac{3}{8}\bar{y}^2 + \frac{1}{10}\bar{y}^{5/2} - \frac{1}{48}\bar{y}^3 + \cdots\}, \text{ for } \bar{y} \ll 1. \tag{3.3}$$

One numerical method used to solve the eigenvalue problem (3.2) is to start the integration procedure at a small value of $\bar{y} = \delta$, say. Then for non-neutral solutions, for example, we can fix β and guess α, complex, and find two independent solutions for $\bar{p}$ corresponding

8

to $(a_1, a_2) = (1, 0), (0, 1)$ using a standard 4th order, 4 stage Runge-Kutta scheme. The integration is continued to a large value of $\bar{y}, y_\infty$ say, where $\bar{p} \sim \exp[-(\alpha^2(1 - M_\infty^2) + \beta^2)^{1/2}\bar{y}]$ and the two solutions $\bar{p}_1$ and $\bar{p}_2$ are combined in the form

$$\bar{p} = P\bar{p}_1 - \frac{2}{3}\tau\alpha^2\bar{p}_2, \tag{3.4}$$

where P is defined by (3.2d). Without loss of generality we may choose $A = 1$. This system is iterated until the condition

$$\bar{p}'(y_\infty) + \overline{\lambda}\bar{p}(y_\infty) = 0 \tag{3.5}$$

is satisfied, where $\overline{\lambda} = (\alpha^2(1 - M_\infty^2) + \beta^2)^{1/2}$ with $Re(\overline{\lambda}) > 0$. In another method, to avoid the possibility of exponential growth in the numerical solution on the interval (δ, y_∞), the solution of (3.2a) can be found first from $\bar{y} = \delta$ to $\bar{y} = y_0$ ($y_0 = 1$, for instance), choosing $A = 1$ and using the asymptotic behavior of (3.3) as initial conditions. Additionally a solution of (3.2a) may be found from $\bar{y} = y_\infty$ to $\bar{y} = y_0$ using the exponential decaying behavior at $\bar{y} = y_\infty$, and choosing the constant multiplying the solution so that the two solutions are continuous at $\bar{y} = y_0$. The condition that $\bar{p}$ and $\bar{p}'$ are continuous at $\bar{y} = y_0$ is sufficient to determine the complex eigenvalue α for fixed β, M_∞, τ and Ω. In some instances, to aid convergence, a further method was used where it was found useful to map $(0, \infty)$ onto $(0, 1)$ by use of the transformation $\bar{y} = \tan(\pi s/2)$. The method of solution in this case can be either of the two methods described above, since the asymptotic behavior of the transformed equation of (3.2a) as $s \to 0+$ and $s \to \infty$ is unchanged (simply replace $\bar{y}$ by $\tan(\pi s/2)$). Each method described above was found to give results consistent with the other two. Each scheme was used with different values of δ and the step length for the Runge-Kutta integration scheme to test for convergence.

Neutral and unstable solutions of (3.2) were found by using the numerical methods described above and are shown mainly in Figure 2; see also in Figures 3,4 later. The behavior of the solutions was followed as the (real) frequency Ω was increased. The neutral solutions were obtained for two-dimensional and three-dimensional disturbances. It was found useful to plot the neutral curves for fixed values of β/α. Figure 2(a) shows the neutral values of τ and Ω for $M_\infty = 0.5$ and $\beta/\alpha = 0, 1, 2, 4$. We see that τ decreases as Ω increases. The neutral solutions for supersonic flows differ depending on whether $\beta/\alpha - (M_\infty^2 - 1)^{\frac{1}{2}}$ is positive or negative. (The situation with $\beta/\alpha = (M_\infty^2 - 1)^{\frac{1}{2}}$ is not addressed here.) Figure 2(b) shows neutral values of τ and Ω for $M_\infty = 2$ and $\beta/\alpha = 1.75, 1.5, 1.25, 1, 0$. For $\beta/\alpha > (M_\infty^2 - 1)^{\frac{1}{2}}$ the solution for $\bar{p}$ is real and decays exponentially as $\bar{y} \to \infty$. For $\beta/\alpha < (M_\infty^2 - 1)^{\frac{1}{2}}$ we allow outgoing traveling waves and so $\bar{p}$ is complex and has a purely oscillatory behavior as $\bar{y} \to \infty$. These two different types of solution produce different forms of the neutral curves as shown in Figure 2(b). For $\beta/\alpha > (M_\infty^2 - 1)^{\frac{1}{2}}$ ($\beta/\alpha = 1.75$) there is no solution for large

9

values of both τ and Ω. For $\beta/\alpha < (M_\infty^2 - 1)^{\frac{1}{2}}$ there exists a cut-off value of Ω for each value of β/α below which there are no solutions. As Ω increases from the cut-off value, on the upper curve, τ reaches a local maximum and then decreases to a local minimum as Ω increases further. Beyond the local minimum the curve has no more turning points and τ continues to increase as Ω increases. We note that the upper curve for the 2D case $\beta/\alpha = 0$ does have this behavior but because of the scale of Figure 2(b) it is not immediately apparent. The lower curves become almost coincident as Ω increases, including the cases $\beta/\alpha > (M_\infty^2 - 1)^{\frac{1}{2}}$ for which τ continues to grow as Ω becomes increasingly small. Thus we see that there exist neutral (and hence unstable) solutions of (3.2), over a range of τ, for all values of Ω for $\beta/\alpha > (M_\infty^2 - 1)^{\frac{1}{2}}$ or for any subsonic case, but there is a cut-off value of Ω for each value of β/α for which $\beta/\alpha < (M_\infty^2 - 1)^{\frac{1}{2}}$ where no neutral (or unstable) solutions exist for Ω below this value. Figure 2(c) shows neutral values of α and Ω for $M_\infty = 2$ and $\beta/\alpha = 1.5, 1.25, 1, 0$. The curves for $\beta/\alpha > (M_\infty^2 - 1)^{\frac{1}{2}}$ for the supersonic case and for any subsonic case are also shown. They are only present on the upper curve where the different solutions are indistinguishable. For $\beta/\alpha > (M_\infty^2 - 1)^{\frac{1}{2}}$ and also for $M_\infty < 1$ the pressure $\bar{p}$ is real, hence, from (3.2d) P must be real also. This implies the well known result that $\xi_0 = -2.298i^{\frac{1}{3}}$ and $i^{-\frac{1}{3}} Ai'(\xi_0)/\kappa(\xi_0) = 1.001$. The definition of ξ_0 from (2.15d) determines α for these cases. We find that $\alpha = (\Omega/2.298)^{\frac{3}{2}}$. Hence, for the cases where this solution is valid, α is independent of M_∞, β and τ. The two branches of the neutral curves shown in Figure 2(c) correspond to the asymptotic solutions described later in sections 3(b) and 3(c).

The effects of increasing the cooling of the surface were investigated by decreasing τ for two-dimensional, three-dimensional, subsonic and supersonic (for moderate values of M_∞) disturbances. The trends were found to be the same in all of these cases, namely that decreasing τ increases the growth rate of the unstable solution. This is shown, for example, in Figure 2(d) for $M_\infty = 0.5$, $\beta = 1$ and $\tau = 0.1, 0.05, 0.02$, where the growth rate $-Im(\alpha)$ is plotted against Ω. We observe that the growth rate increases significantly as τ decreases (i.e. when the wall is cooled more). This suggests a large destabilization of the basic flow as the wall cooling is increased. The results for $M_\infty = 0.5$ and $\beta = 0$ for $\tau = 0.1, 0.05, 0.02$ are graphically identical to the respective results for $\beta = 1$ shown in Figure 2(d). The real part of α is very large for these solutions for small values of τ. Figure 2(e) shows the growth rate $-Im(\alpha)$ as a function of Ω for $M_\infty = 2$, $\beta = 1$ and $\tau = 0.1, 0.05, 0.02$. The solutions have the same behavior as those shown in Figure 2(d) for $M_\infty = 0.5$ with the growth rates appearing to be slightly smaller for $M_\infty = 2$ compared to those for $M_\infty = 0.5$. Again, the corresponding solutions for $M_\infty = 2$ and $\beta = 0$ are virtually the same as those for $M_\infty = 2$ and $\beta = 1$ for the values of τ shown in Figure 2(e).

For large values of τ the solutions approached those of Smith (1987) as expected (see

also (c) below]. For subsonic flows as τ increases the solutions for $Im(\alpha)$ have the same behavior as those shown in Figure 2(d) with the growth rates continuing to decrease as τ increases. This behavior is found to hold for very large values of τ. This is illustrated in Figure 2(f) where $-Im(\alpha)$ is plotted against Ω for $M_\infty = 0.5$, $\beta = 0$ and $\tau = 0.4, 0.5, 1$. If the corresponding curves for $\beta = 1$ were to be added to Figure 2(f) they would be indistinguishable. Figure 2(g) shows $-Im(\alpha)$ as a function of Ω for $M_\infty = 0.5$ and $\beta = 0$ and $\beta = 1$ for $\tau = 10, 20$. The solutions for $\beta = 1$ and $\beta = 0$ are now distinct, with the solutions for $\beta = 0$ having larger growth rates, the difference increasing as τ increases. We note that as Ω increases from zero the three-dimensional mode occurs first.

For supersonic flows, as expected from the neutral curves shown in Figure 2(b), the structure of the eigenvalue α changes as τ increases. An example of this is shown in Figure 2(h) where $-Im(\alpha)$ is plotted against Ω for $M_\infty = 2$ and $\beta = 0$ for $\tau = 0.4, 0.5, 1$. For $0 < \tau \leq 0.4$ there is one neutral point at a small value of Ω. For $0.4 < \tau < 1$ there are 3 neutral points and for $\tau \geq 1$ only the neutral point at the largest value of Ω persists. Figure 2(i) shows $-Im(\alpha)$ as a function of Ω for larger values of τ, namely for $M_\infty = 2$, $\beta = 0$ and $\tau = 5, 10, 17$. For the range of τ shown in Figures 2(h) and 2(i) the solutions for $\beta = 1$ are very close to those shown for $\beta = 0$. As τ increases the growth rate continues to decline.

To summarize the results of the computational study for moderate values of M_∞ we can make the following general statements. As the amount of wall cooling is increased (i.e. as τ is decreased) the growth rates increase for two-dimensional and three-dimensional perturbations, irrespective of whether the flow is subsonic or supersonic. Moreover, as τ is increased, for subsonic flows no significant three-dimensional effects are noticeable until $\tau \geq 10$, with the growth rates here being larger for two-dimensional perturbations. On the other hand, for supersonic flows with $\beta/\alpha < (M_\infty^2 - 1)^{\frac{1}{2}}$ there is very little difference between the solutions for two-dimensional and three-dimensional flows. Again, for a fixed value of τ the growth rates for subsonic flow are larger than those for supersonic flow.

We also note that, here and below, multiple modes may be present but these have not been detected as yet.

For large values of M_∞ the mean flow becomes different in structure. In particular, from the Howarth-Dorodnitsyn transformation, $T_0 \sim M_\infty^2$ so that $\overline{y} \sim M_\infty^2$, while $U_0 \sim O(1)$. We do not present solutions for large Mach number but below is an outline of a representative problem to be solved in this case. For large M_∞ we write

$$\overline{y} \quad \overline{Y} M_\infty^2, \tag{3.6}$$

and then

$$[U_0, T_0, M_0, \alpha] \quad [\overline{U}_0(\overline{Y}), M_\infty^2 \overline{T}_0(\overline{Y}), \overline{M}_0(\overline{Y}), M_\infty^2 \overline{\alpha}], \tag{3.7}$$

11

instead of (3.1a,b), with the over-barred variables now being typically of order one. The equation (2.15) therefore becomes

$$\overline{p}_{\overline{Y}\overline{Y}} - \frac{2\overline{M}_{0\overline{Y}}}{\overline{M}_0}\overline{p}_{\overline{Y}} - [\overline{\alpha}^2(1 - \overline{M}_0^2) + \overline{\beta}^2]\overline{p} = 0, \tag{3.8}$$

for $0 < \overline{Y} < \overline{Y}_\infty$, where the scaled boundary-layer edge $\overline{Y}_\infty$ is finite in this regime, $\overline{M}_0 \equiv \overline{U}_0\overline{T}_0^{-\frac{1}{2}}$, and $\beta = M_\infty^{-2}\overline{\beta}$. The boundary conditions near the cooled surface likewise remain intact, to leading order, with z, P, A also scaled appropriately with respect to M_∞, taking account also of the extra factors such as c_1, c_2 involved in the scales of section 2. In particular, the typical wall-cooling factor τ required now increases like $M_\infty^{\frac{6}{5}}$. A logarithmically thin extra layer near $\overline{Y} = \overline{Y}_\infty$ adjusts the solution from T_0 being $O(M_\infty^2)$ (as above) to being unity as required in the free stream, and so the profiles $\overline{U}_0$, $\overline{T}_0$ are to satisfy the conditions $\overline{U}_0 \to 1$, $\overline{T}_0 \to 0$ as $\overline{Y} \to \overline{Y}_\infty-$ and $\overline{U}_0 \propto \overline{Y}^{\frac{1}{2}}$, $\overline{T}_0 \propto \overline{Y}^{\frac{1}{2}}$ as $\overline{Y} \to 0+$.

(b) Small τ: towards severe cooling

In line with the computational results, it is suggested that for small values of τ the disturbance $\overline{y}$ - scale contracts. So U_0, T_0 are approximately like $\overline{y}^{1/2}$, M_0 is small of order $\overline{y}^{1/4}$ for M_∞ of $O(1)$, cf. later, and therefore (2.15a) suggests that α is $O(\overline{y}^{-1})$, as is β. The unknown $\overline{y}$-scale is then fixed in terms of τ by comparing the typical size of P/A from (2.15c) with that inferred from (2.15d), given that ξ_0 is expected to remain typically $O(1)$ for instability. The implied small-τ response therefore has

$$\overline{p} = \hat{p}(\hat{y}) + \cdots, \quad \overline{y} = \tau^{6/5}\hat{y}, \tag{3.9a}$$

$$(\alpha, \beta) = \tau^{-6/5}(\hat{\alpha}, \hat{\beta}) + \cdots, \quad \Omega = \tau^{-4/5}\hat{\Omega} + \cdots, \tag{3.9b}$$

$$P = \hat{P} + \cdots, \quad A = \tau^{-2/5}\hat{A} + \cdots. \tag{3.9c}$$

This reduces (2.15) to the equation

$$\hat{p}_{\hat{y}\hat{y}} - \frac{\hat{p}_{\hat{y}}}{2\hat{y}} - (\hat{\alpha}^2 + \hat{\beta}^2)\hat{p} = 0, \tag{3.10a}$$

for $\hat{p}$, subject to

$$\hat{p}(\infty) = 0, \quad \hat{p} - \hat{P} - \frac{2}{3}\hat{\alpha}^2\hat{A}\hat{y}^{3/2} \text{ as } \hat{y} \to 0+, \tag{3.10b, c}$$

and

$$\hat{P}/\hat{A} - (1 + \hat{\beta}^2/\hat{\alpha}^2)^{-1}(i\hat{\alpha})^{1/3}Ai'(\hat{\xi}_0)/\kappa(\hat{\xi}_0), \tag{3.10d}$$

where $\hat{\xi}_0 = -i^{1/3}\hat{\Omega}/\hat{\alpha}^{2/3}$. Here the solution of (3.10a,b) can be obtained analytically,

$$\hat{p} - d_1\hat{y}^{3/4}K_{\frac{3}{4}}(\hat{\hat{y}}) \text{ with } \hat{\hat{y}} = (\hat{\alpha}^2 + \hat{\beta}^2)^{1/2}\hat{y}, \tag{3.11a}$$

12

d_1 is a constant, $K_{3/4}$ is the Bessel function in the standard notation, and then (3.10c) requires that

$$\hat{P}/\hat{A} = \frac{2\pi\hat{\alpha}^2}{(\Gamma(\frac{1}{4}))^2(\hat{\alpha}^2 + \hat{\beta}^2)^{3/4}} \quad , \tag{3.11b}$$

from the behavior of the Bessel function at small $\hat{y}$. So the coupling with (3.10d) leads to the reduced eigenrelation

$$\frac{Ai'(\hat{\xi}_0)}{\kappa(\hat{\xi}_0)} = \frac{2\pi}{(\Gamma(\frac{1}{4}))^2}(i\hat{\alpha})^{1/3}(\hat{\alpha}^2 + \hat{\beta}^2)^{1/4}, \tag{3.11c}$$

between $\hat{\alpha}, \hat{\Omega}$. The solution for $Re(\alpha)$ and $Im(\alpha)$ from (3.11c) are plotted in Figures 3(a) and 3(b), respectively, for $\beta = 1$ and $\tau = 0.1, 0.05, 0.02$. These are seen to agree well with the full computations at small values of τ; see also in Figures 2(d) and 2(e). In order to illustrate this agreement Figures 3(c) and 3(d) show $Re(\alpha)$ and $Im(\alpha)$ for $\tau = 0.05$, $\beta = 0$, for $M_\infty = 0.5$ and $M_\infty = 2$ from the full computations along with the result of (3.11c). The agreement is seen to be very close when Ω is not very large.

It is interesting that the small-τ response here is independent of the Mach number, as might be expected for disturbances focussed near the surface. This is because the effective Mach number M_0 is small, so that the contribution M_0^2 in (2.15a) is negligible, although the instabilities that are found to exist do remain temperature- and velocity-driven through the ratio $M_{0\bar{y}}/M_0$ operating in (2.15a). The property that these extra-cooled-surface instabilities exist at any Mach number, and for both 2D and 3D modes, contrasts with the situation for the less cooled surfaces corresponding to large τ or to the earlier regime of (2.1), where, in the supersonic range, instabilities occur only for sufficiently oblique modes directed outside the wave-Mach-cone: see (c) below. Thus the cooling now destabilizes a range of previously stable viscous modes. Moreover, the de-stabilization is very marked, for all the viscous modes, in the sense that the spatial growth rates produced are much larger than encountered before. Indeed, the growth rates appear to exceed those of purely inviscid modes (see also section 5). The small-τ response leads on to the new structure investigated in section 4.

(c) Large τ and the cut-off

The clue to the behavior at large τ, associated with less cooled surfaces, is found in high-frequency properties. Thus when Ω is large, at $O(1)$ values of τ first, the outer solution of (2.15a) takes the form

$$[\bar{p}, P, A, \alpha, \beta, M_0] = [\hat{p}, \hat{P}, \Omega^{-1/3}\hat{A}, \Omega^{2/3}\hat{\alpha}, \Omega^{2/3}\hat{\beta}, O(\Omega^{-1/6}\hat{y}^{1/4})] + \cdots, \quad \bar{y} = \Omega^{-2/3}\hat{y}, \tag{3.12a}$$

concentrated again near the wall. So $\hat{p}$ satisfies the equivalent of (3.10a), subject again to

(3.10b,c). Here however the sublayer relation is simply

$$\hat{P}/\hat{A} = \hat{\alpha}^{-1}(1 + \hat{\beta}^2/\hat{\alpha}^2)^{-1}, \tag{3.12b}$$

as $|\xi_0|$ is large for these high frequencies. Hence we have the result

$$\hat{\alpha} = (\Gamma(\frac{1}{4}))^{4/3}/(2\pi\tau)^{2/3}, \tag{3.12c}$$

for the 2D example [the 3D version has an extra factor $(1 + \hat{\beta}^2/\hat{\alpha}^2)^{-1/6}$ on the right-hand side], giving neutral stability at leading order. This result is essentially an inviscid one since the asymptote $-\xi_0$ for Ai'/κ in (3.10d), used in (3.12b), corresponds to an inviscid limit, and, like that in (b) above, the present result applies for all Mach numbers.

Closer inspection then shows that the high-frequency structure and results (3.12b,c) continue to hold for all τ, provided that $\Omega \gg \tau^{-4/5}$ and $\Omega \gg \tau$, the former to keep $|\xi_0|$ large and the latter to keep α large (and $\bar{y}$ small), as supposed above. The former restriction is associated more with decreasing τ since (b) comes into play exactly when Ω reaches the order $\tau^{-4/5}$ and thus provides a match. The other restriction is connected with the large-τ behavior below. Also, we note that higher-order contributions in inverse powers of Ω bring in the second term in Ai'/κ, which is a viscous and de-stabilizing effect, such that there exists instability for any value of τ, at sufficiently high frequencies.

To complete the picture at large τ, then, we move on to consider Ω values of order τ (Figure 4). The properties are mainly inviscid again since $|\xi_0|$ is large, in fact comparable with Ω, as

$$\tau \sim \Omega\hat{\tau} \text{ with } \alpha, \beta = O(1), \quad \bar{y} = O(1), \tag{3.13a}$$

to leading order. The dominant equation to solve is therefore exactly (2.15a), with the constraint (2.15b) still, but (2.15c) becomes

$$\bar{p} \sim P[1 - \frac{2}{3}\hat{\tau}\alpha(\alpha^2 + \beta^2)\bar{y}^{3/2}] \text{ as } \bar{y} \to 0+, \tag{3.13b}$$

because the sublayer response gives here $\Omega A = (\alpha^2 + \beta^2)P/\alpha$. The computed solution of (2.15a,b) with (3.13b) is presented in Figure 4(a) along with comparisons with the computations of section 3(a) and the solution from (3.12). At small $\hat{\tau}$, corresponding to reduced τ and/or larger Ω values, there is a match with (3.12) as expected, for any Mach number. Figures 4(b,c,d) show solutions from the computations of section 3(a) for large τ with $M_\infty = 2$ and $\beta = 0$. In Figures 4(e,f,g) we show $\hat{\tau}$ as a function of Ω along the neutral curves for $M_\infty = 2$ and $\beta = 0, 1, 1.5$, as shown in Figure 2(b). We see that for the branch $\tau \gg 1$ and $\Omega \gg 1$ $\hat{\tau}$ decreases as Ω increases so there will be a cut-off value of $\hat{\tau}$ above which no unstable solutions exist. As $\hat{\tau}$ increases the solution becomes Mach-number dependent, and

14

this is *especially so at large* $\hat{\tau}$ *where the subsonic realm remains always unstable but the* supersonic realm becomes stable within the wave-Mach-cone $\beta < \alpha(M_\infty^2 - 1)^{1/2}$, including the 2D case. The cut-off here, for the less oblique supersonic modes, is profile-dependent but occurs at an $O(1)$ crossover or neutral value of $\hat{\tau}$. That yields the predictions (in line with the computations just mentioned and with those of Figure 2)

$$\left.\begin{array}{ccc} \Omega - neutral & \propto & \tau \\ \\ \Omega - max & \propto & \tau \end{array}\right\} \text{ as } \tau \to \infty, \qquad (3.14a,b)$$

for $M_\infty > 1$ and waves directed inside the wave-Mach-cone. This behavior is illustrated in Figure 4(h) where $\Omega - max$ is plotted as a function of τ for $\beta = 0$ and $M_\infty = 0.5$. The frequency $\Omega = \Omega - max$ is that at which the maximum growth rate occurs. In contrast, analysis for the more oblique supersonic modes and for the subsonic ones shows that at large τ the outer solution develops a double structure, leading to the typical response

$$\alpha \sim (1 - M_\infty^2)^{1/4}/\hat{\tau}^{1/2}, \qquad (3.15)$$

for the 2D subsonic case for instance. This confirms the suggestion of the computations, that the result (3.14b) in fact holds for all the supersonic and subsonic modes, whereas the subsonic and more oblique supersonic ones retain instability at large $\hat{\tau}$ (i.e. $\Omega << \tau$), as opposed to (3.14a).

The double structure just mentioned leads to the final phase for the latter modes, namely when Ω falls to $O(\tau^{-1/2})$. Then $|\xi_0|$ decreases to $O(1)$ since

$$(\alpha, \beta) \sim \tau^{-3/4}(\alpha_*, \beta_*) \text{ with } \Omega \sim \tau^{-1/2}\Omega_*, \qquad (3.16)$$

from (3.15), with $\alpha_*, \beta_*, \Omega_*$ of order unity, so the fully viscous sublayer relation (2.15d) is re-installed. Moreover, the outer double structure produces the two $\bar{y}$-scales $O(\tau^{3/4})$ and $O(1)$, the former giving a potential-flow character and the latter a profile-dependent displacement effect, leading to the relation $P = \alpha_* A \tau^{-3/4} (1 - M_\infty^2)^{-1/2}$ for subsonic 2D modes for instance. Coupling this with (2.15d), then, we obtain the eigenrelation

$$\frac{\kappa(\xi_0)}{Ai'(\xi_0)}(i\alpha_*)^{1/3} = \frac{(1 - M_\infty^2)^{1/2}}{\alpha_*}, \qquad (3.17)$$

between α_*, Ω_*, again for the 2D subsonic case as an example. There are two main points here. First, the relation (3.17), which agrees with (3.15) at large Ω_* as required, produces a maximum growth rate at an $O(1)$ value (approx. 4) of Ω_* and neutral stability at a smaller $O(1)$ value (Ω_* approx. 2.3), thus giving rise to the predictions

$$\left.\begin{array}{ccc} \Omega - neutral & \sim & \tau^{-1/2} \\ \\ \Omega - max & \sim & \tau^{-1/2} \end{array}\right\} \text{ as } \tau \to \infty. \qquad (3.18a,b)$$

15

These again appear to be consistent with the computations at large τ, as shown in Figure 4(i) where $\Omega - max$ is shown as a function of τ for $\beta = 0$ and $M_\infty = 2$. Second, the entire structure in this regime, and the results (3.16) - (3.18), match directly with the earlier triple-deck case (see (2.1)). For instance, the wavelength $O(Re^{-1/2}\alpha^{-1})$ increases to $O(Re^{-3/8})$ when T_w is raised to $O(1)$, since then $\tilde{T}_w \propto \tau^{1/2} \rightarrow 0(Re^{1/12})$ and $\alpha \rightarrow 0(Re^{-1/8})$ from (3.16). Similar matching holds with regard to (3.17), (3.18), for 2D and 3D subsonic or supersonic modes (Smith 1987).

The splitting of the neutral curves for the different cases, and the production of two local maxima (and mounds of instability) in certain cases, via (3.14), (3.18), reflects the emergence of two major types of instability when the surface temperature increases. These are the viscous-inviscid triple-deck type (of (2.1) ff), with which (3.18) connects [see comments above], and the inviscid compressible-Rayleigh type, which are implied by (3.14). In the latter case, raising T_w back to $O(1)$ corresponds to $\tilde{T}_w$ increasing to $O(Re^{1/12})$, hence τ to $O(Re^{1/6})$, and so the Ω's in (3.14) become $O(Re^{1/6})$ also, meaning that the time scale t becomes $O(Re^{-1/2})$, from (2.8). This t-scale, the x-,y-scales of order $Re^{-1/2}$, and the increased wavespeed of order unity, all coincide with the compressible Rayleigh scales : see also section 5.

Finally here, a combination of the small-τ features in (b) above and those for large τ in (3.14) indicates the existence of an $O(1)$ value of the effective surface temperature at which Ω-neutral is a minimum, for the supersonic 2D and less inclined 3D waves. This is as shown in the figures. The corresponding Ω value in the 2D case for instance represents a critical value of the scaled frequency, below which 2D modes remain stable, in supersonic flow, and above which they are unstable for a range of surface temperatures.

4. THE SEVERE-COOLING REGIME

This regime has much reduced surface temperatures and its structure is inferred from the properties found in section 3(b). Thus for small τ the characteristic thickness of the outer tier deceases like $\tau^{6/5}$, as does the streamwise length scale, while the buffer thickness which is proportional to $\tilde{T}_w^2$ decreases like τ in view of (2.12a). Along with this, the representative viscous-tier thickness falls as $\alpha^{-1/3}\tilde{T}_w$ because of the scaling in (2.7) and the definition of ξ_0. The unscaled thicknesses are therefore of the orders $Re^{-1/2}\tau^{6/5}$, $Re^{-2/3}\tau$, $Re^{-3/4}\tau^{9/10}$ respectively.

The severe-cooling regime arises when any two of the last three thicknesses mentioned become coincident. For instance if the buffer thickness coincides with the viscous-tier thickness then $\tau \sim Re^{-5/6}$, giving

$$T_w \sim Re^{-1/2} \tag{4.1}$$

16

as the typical surface temperature here. At that stage the other thickness above also becomes comparable with the other two, and so a single-tier structure is expected to apply for severe surface cooling. In effect the original main tier and buffer layer now enter the viscous sublayer. The corresponding streamwise length scale is $O(Re^{-3/2})$ which is relatively tiny and coincides with the inner-tier thickness where $y \sim Re^{-3/2}$ and viscous compressible effects are felt. The corresponding velocity, pressure, temperature, density and viscosity scales can be worked out likewise. The resultant governing equations for the severely-cooled flow are in effect the unsteady compressible Navier-Stokes equations,

$$\rho_t + (\rho u)_x + (\rho v)_y + (\rho w)_z = 0, \tag{4.2a}$$

$$\rho[\partial_t + u\partial_x + v\partial_y + w\partial_z]u = -p_x + \partial_x[2\mu u_x + (\mu' - \frac{2}{3}\mu)\nabla.\underline{V}] + \partial_y[\mu(u_y + v_x)] + \partial_z[\mu(w_x + u_z)], \tag{4.2b}$$

$$\rho[\partial_t + u\partial_x + v\partial_y + w\partial_z]v = -p_y + \partial_y[2\mu v_y + (\mu' - \frac{2}{3}\mu)\nabla.\underline{V}] + \partial_z[\mu(v_z + w_y)] + \partial_x[\mu(u_y + v_x)], \tag{4.2c}$$

$$\rho[\partial_t + u\partial_x + v\partial_y + w\partial_z]w = -p_z + \partial_z[2\mu w_z + (\mu' - \frac{2}{3}\mu)\nabla.\underline{V}] + \partial_x[\mu(w_x + u_z)] + \partial_y[\mu(v_z + w_y)], \tag{4.2d}$$

$$\rho[H_t + uH_x + vH_y + wH_z] = \nabla.(k\,\mathrm{grad}\,T + \underline{\tau}\,\underline{u}), \tag{4.2e}$$

$$H = \frac{1}{2}(u^2 + v^2 + w^2) + \frac{p}{\rho}, \quad \mu = CT, \quad p = \mathcal{R}\rho T, \tag{4.2f,g,h}$$

where H is the enthalpy, $\underline{\tau}$ is the stress tensor and σ is the Prandtl number. Here again the nonlinear interaction is set up first, with small perturbations then being governed by the linearized version. The basic undisturbed flow has $u = \hat{T}_w c_2 c_1^{-1}[(1 + 2c_1 y)^{1/2} - 1]$ and $T = \hat{T}_w(1 + 2c_1 y)^{1/2}$, as in (2.3) in effect, and the boundary conditions on (4.2) include

$$u = v = w = 0, \quad T = \hat{T}_w, \text{ at } y = 0, \tag{4.3a}$$

$$u \sim \hat{T}_w \frac{c_2}{c_1}[(1 + 2c_1 y)^{1/2} - 1], \quad T \sim \hat{T}_w(1 + 2c_1 y)^{1/2}, \quad p \to 0, \text{ as } y \to \infty, \tag{4.3b}$$

where $\hat{T}_w$ is the scaled surface temperature.

The main difference from the previous cooling regime is that the viscous Navier-Stokes motion is now fully compressible (and single-structured), contrasting with the quasi-incompressible sublayer properties holding before. The scales involved are extreme but they can be verified from an order-of-magnitude argument. Further, the present flow structure applies for any Mach number, in line with the closeness of the Navier-Stokes structure to the surface; and both the spatial and temporal growth rates induced for small perturbations are an order-of-magnitude larger than those found previously for inviscid modes, because of the tiny scales involved here.

17

This new predominance of the viscous modes is due physically to the high surface shear stresses and surface heat transfer rates that the cooling of the surface provokes. The same comment applies to section 3(b). The precise behavior is of course dependent on the temperature-viscosity law in operation (unlike the law-independent triple-deck case of (2.2)), but the same qualitative behavior seems likely to hold in general, for the same physical reasons. Linearized or nonlinear solutions in this regime could therefore be of some interest, as $\hat{T}_w$ is varied.

5. ON INVISCID MODES ON COOLED SURFACES

The pure inviscid stability of compressible boundary layers is controlled by the compressible Rayleigh equation

$$\bar{p}'' - \frac{2\overline{M}'}{\overline{M}}\bar{p}' - [\alpha^2(1 - \overline{M}^2) + \beta^2]\bar{p} = 0, \tag{5.1a}$$

for the pressure perturbation, with the length scales as for the main tier in section 2 but now the wavespeed c is $O(1)$, so that

$$\overline{M} \equiv (U_0 - c)M_\infty T_0^{-1/2}, \tag{5.1b}$$

cf. (2.15a). The boundary conditions are to match with the undisturbed incident free stream and to satisfy the tangential-flow surface condition,

$$\bar{p} \to 0 \text{ [or outgoing waves] as } \bar{y} \to \infty, \tag{5.1c}$$

$$\bar{p}' = 0 \text{ at } \bar{y} = 0, \tag{5.1d}$$

respectively. Computational solutions of (5.1) are given by Mack, Malik and others (see references in §1) including some investigations for cooled surfaces. The investigations trace the effects of gradual cooling on the originally un-cooled inviscid modes and find some interesting features. There is no significant change of scale however. The present investigation focuses mostly on new inviscid modes involving substantial scale changes and, in particular, much increased growth rates.

The main factor for cooled surfaces where T_w is small is the development of the $O(T_w^2)$ sublayer described by (2.3), associated with high wall shear and temperature gradient. The previous investigations mentioned above neglect the sublayer in a sense and seek solutions of (5.1) on the scale $\bar{y}$ of $O(1)$. Here, in contrast, we find significant effects arising when the sublayer plays an active role. We concentrate now on the two different cases.

The first type addressed has $c \sim T_w^2$ and $\alpha \sim T_w$. This is suggested by the form of $\overline{M}$ in the sublayer, namely $O(T_w^2)$ [...] (from 5.1b with 2.3a), and by

the balance of terms in (5.1a). So $\overline{M}$ is large in the sublayer and (5.1a) reduces to

$$\overline{p}'' + \frac{\overline{p}'}{2\hat{y}} + \frac{k^2\overline{p}}{\hat{y}^{1/2}} = 0, \qquad (5.2a)$$

where $\hat{y} = \hat{y} + (2c_1)^{-1}$, the parameter $k = \alpha c M_\infty (2c_1)^{-1/4} T_w^{3/2}$ is $O(1)$ and c_1 is the heat-transfer factor defined in (2.3b). Here (5.2a) becomes Airy's equation in terms of the variable $s = \hat{y}^{1/2}$ and so the constraints (5.1c,d) lead to the eigenrelation

$$-2iAi(-(4k^2)^{1/3}) + Bi(-(4k^2)^{1/3}) = 0 \qquad (5.2b)$$

for k. This has no real roots. All the (complex) roots give damped waves in fact, but this type of mode serves to suggest the new scales for the second type of surface-cooled mode. Here c reduces to $O(T_w^{1/2})$, and $\alpha \sim T_w^{-2}$, as implied by the first type, and this brings in a new effect since now $\overline{M}$ is of order unity. Thus if $c = T_w^{1/2}\tilde{c}$ and $\alpha = T_w^{-2}\tilde{\alpha}$ then $\overline{M} \propto \hat{y}^{-1/4}$ to leading order and (5.1a) becomes

$$\overline{p}'' + \frac{\overline{p}'}{2\hat{y}} + \tilde{\alpha}^2 [\frac{\tilde{c}^2 M_\infty^2}{(2c_1\hat{y})^{1/2}} - 1]\overline{p} = 0. \qquad (5.3a)$$

For $\tilde{\alpha}$ real, the substitution $\hat{y}^{1/2} = \tilde{c}^2 M_\infty^2/(8c_1)^{1/2} + \tilde{s}/(2\tilde{\alpha}^{1/2})$ converts (5.3a) to the parabolic cylinder equation

$$\overline{p}_{\tilde{s}\tilde{s}} - (\frac{\tilde{s}^2}{4} - \tilde{\beta})\overline{p} = 0, \qquad (5.3b)$$

where $\tilde{\beta} = \tilde{\alpha}\tilde{c}^4 M_\infty^4/(8c_1)$ and the boundary conditions are $\overline{p}(\infty) = 0, d\overline{p}/d\tilde{s} = 0$ at $\tilde{s} = (2-\tilde{c}^2 M_\infty^2)\tilde{\alpha}^{1/2}/(2c_1)^{1/2}$. The solution is therefore the parabolic cylinder function $\overline{p} = U(a,\tilde{s})$ with $a = -\tilde{\beta}$ (see Abramowitz & Stegun (1964)), for the outer constraint, while the inner constraint requires that $\tilde{s} = x_n$ where x_n are the roots of

$$U'(a, x_n) = 0. \qquad (5.3c)$$

The above reference shows that there do exist some roots with a being negative, $\tilde{\beta}$ positive, as required, occurring for positive x_n. For those roots the values of $\tilde{\alpha}, \tilde{c}$ then follow from the relations

$$(2 - \tilde{c}^2 M_\infty^2)\tilde{\alpha}^{1/2}/(2c_1)^{1/2} = x_n, \qquad (5.4a)$$

$$\tilde{\alpha}\tilde{c}^4 M_\infty^4/(2c_1) = 4\tilde{\beta}. \qquad (5.4b)$$

The resulting wave speeds $\tilde{c}$ are all real, given by

$$\tilde{\alpha}^{1/2} = (\tilde{\beta}^{1/2} + x_n/2)(2c_1)^{1/2}, \quad M_\infty \tilde{c} = 2(2 + x_n/\tilde{\beta}^{1/2})^{-1/2}, \qquad (5.5a,b)$$

19

where the first equation fixes $\tilde{\alpha}$, the second $\tilde{c}$. Hence this new type, which is a temperature-driven mode because of the form of $\overline{M}$, produces new inviscid neutral modes.

The third case has c decreased still further, to $O(T_w)$, which reinstates the influence of the velocity profile U_0 as well as the temperature at leading order. For, if $c = T_w \hat{c}$, $\alpha = T_w^{-2} \hat{\alpha}$, then $\bar{M} = T_w^{1/2} \tilde{M}$ is small and the controlling equation becomes

$$\bar{p}'' - \frac{2\tilde{M}'}{\tilde{M}}\bar{p}' - \alpha_1{}^2\bar{p} = 0, \tag{5.6a}$$

with

$$\tilde{M} = [(y_1{}^{1/2} - 1)2\lambda_1 - \hat{c}]M_\infty y_1{}^{-1/4}. \tag{5.6b}$$

(Here $y_1 \equiv 2c_1\hat{y}$, $\hat{\alpha} \equiv 2c_1\alpha_1$, $2c_1\lambda_1 \equiv c_2$). This can be recast, by setting $y_1{}^{1/2} = \tilde{\mu}(1 + \xi)$, $\tilde{\mu} = 1 + \hat{c}/2\lambda_1$, in the form

$$\xi\bar{p}_{\xi\xi} - 2\bar{p}_\xi - \phi^2\xi(\xi + 1)^2\bar{p} = 0, \tag{5.6c}$$

with

$$\bar{p}(\infty) = 0, \quad \bar{p}_\xi = 0 \text{ at } \xi = \tilde{\mu}^{-1} - 1, \tag{5.6d}$$

where $\phi \equiv 2\alpha_1\tilde{\mu}^2$ acts as the eigenvalue. This third type can be shown to match with the second type, at large $\hat{c}, \tilde{\mu}$, and similar matching occurs between the first and second types. Hence again in this regime neutral modes are produced.

The fourth type of cooled-surface inviscid mode to consider has a structure suggested by the work of section 3(c). Here c is reduced to $O(T_w^2)$ but α is $O(1)$, and the solution of (5.1) takes on a three-tier form. In the bulk of the boundary layer where $\bar{y}$ is $O(1)$, therefore, (5.1a) applies but with c replaced by zero in the definition of $\overline{M}$ in (5.1b), i.e. (2.15a) holds again with $M_0 = U_0 M_\infty / T_0^{1/2}$, and now

$$\bar{p} \sim P - \frac{2}{3}\alpha^2 A^{**}\bar{y}^{3/2} \text{ as } \bar{y} \to 0+, \tag{5.7}$$

where the relation between the constants A^{**} and P has to be found. The next tier, closer to the surface, has $\bar{y} = T_w^2\hat{y}$ along with (2.3), so that to leading order

$$\overline{M} = T_w^{1/2}\hat{M}(\hat{y}): \quad \hat{M} \equiv \frac{c_2[(1 + 2c_1\hat{y})^{1/2} - 1]M_\infty}{c_1(1 + 2c_1\hat{y})^{1/4}}. \tag{5.8a}$$

Now

$$\bar{p} = P + T_w^3 p_1 + \cdots \tag{5,8b}$$

and consequently the first two terms in (5.1a) dominate, giving on integration

$$\frac{dp_1}{d\hat{y}} = -\frac{\alpha^2 A^{**} c_1^{3/2}}{2^{1/2} M_\infty^2 c_2^2}\hat{M}^2, \tag{5.8c}$$

where the coefficient on the right side is chosen to match with (5.7) and we normalize such that $p_1(0) = 0$. Hence $dp_1/d\hat{y}$ decreases like $\hat{y}^3$ at small $\hat{y}$, which leads on to the lowest tier even closer to the surface where $\overline{y} = T_w^3 \tilde{y}$ with $\tilde{y}$ of $O(1)$. There

$$\overline{p} = P + T_w^6 \tilde{p}_1 + \cdots, \tag{5.9a}$$

and the small wavespeed $c = T_w^2 \tilde{c}$ takes effect since

$$\overline{M} = T_w^{3/2} \tilde{M} + \cdots \text{ with } \tilde{M} \equiv (c_2 \tilde{y} - \tilde{c}) M_\infty, \tag{5.9b}$$

from (5.1b) with (2.3a). Hence the governing equation, from (5.1a), is

$$\frac{d^2 \tilde{p}_1}{d\tilde{y}^2} - \frac{2}{\tilde{M}} \frac{d\tilde{M}}{d\tilde{y}} \frac{d\tilde{p}_1}{d\tilde{y}} = \alpha^2 P. \tag{5.9c}$$

The solution for $d\tilde{p}_1/d\tilde{y}$ merging with (5.8b,c) at large $\tilde{y}$ is then

$$\frac{d\tilde{p}_1}{d\tilde{y}} = -\frac{\alpha^2 P}{c_2}(c_2 \tilde{y} - \tilde{c}) - \frac{\alpha^2 A^{**} c_1^{3/2}}{2^{1/2} c_2^2}(c_2 \tilde{y} - \tilde{c})^2, \tag{5.9d}$$

and so the required surface condition (5.1d) is satisfied at $\tilde{y} = 0$ if

$$A^{**} = \frac{2^{1/2} c_2}{c_1^{3/2} \tilde{c}} P. \tag{5.10}$$

This provides the relation for A**, to be substituted into (5.7). The resulting problem for $\overline{p}$, that is, (2.15a,b) with (5.7), (5.10), is equivalent to the one derived and solved numerically in section 3(c): see (3.13b), where the parameter $\hat{\tau}\alpha^3$ involved for the two-dimensional case is in agreement with that inferred from (5.7), (5.10), with account taken of the different temporal scaling in (2.8). Hence the stability properties in subsonic and supersonic flow, for this fourth type, are exactly as given in Figure 4 with the appropriate change of notation. Like all the types described in this section, this new type appears to be quite distinct from any cooled modes found previously.

6. FURTHER COMMENTS

The main conclusion from the present theoretical research [in particular, §§3,5] is that moderate surface cooling can enhance the TS viscous-mode activity to the extent that the spatial growth of the viscous modes can become comparable with, or even exceed, that of inviscid ones, thus reversing the normal order. In addition, the cooling can completely destabilize otherwise stable viscous modes and inviscid modes, at any Mach number, including the production of radiating waves in the supersonic realm. In those two senses, then, cooling of the surface seems very "dangerous" with regard to transition in the compressible boundary layer.

21

The TS growth, when it exceeds that of the pure inviscid modes studied previously, occurs for disturbances which are confined relatively close to the surface, as opposed to the full inviscid ones stretching all the way across the boundary layer. In particular, for all the new modes, the high-heat-transfer sublayer plays a substantial active part in enhancing the viscous growth, through the correspondingly high shear-stress production at the surface. It could be for that reason, i.e. the appearance of multi-structured responses within the boundary layer, that previous theoretical, computational and experimental studies of surface-cooling effects appear to have not detected the new mode properties, although there are other explanations which suggest themselves such as considerable finite-Reynolds-number effects; see also below. Experiments and computations focusing on the possibility of such strong near-surface behavior remain to be done, it seems, and they could be of much interest scientifically and for practical applications. There is some measure of agreement, nevertheless, between the present theory and the Lysenko and Maslov (1984) experiments. Thus the theory predicts that as the temperature ratio T_w falls from the non-cooled regime to the moderate-cooling regime, for first modes at fixed Reynolds number, the typical streamwise wavenumber, α^D say, and the typical frequency, ω^D say, increase as $T_w^{-3/2}$, T_w^{-1} respectively: see §2. So for the 1 to 0.76 decrease in T_w examined in Lysenko and Maslov's Figure 2 the predicted increase in ω^D is by a factor 1.316, which is not inconsistent with the measured increase in the neutral value of ω^D shown in that figure. (See also comparisons for the insulated case in Smith 1987). Similar trends for decreasing T_w are observed in their Figure 5. Again, Lysenko and Maslov's Figure 4 has a case of a 1 to 0.79 decrease in T_w, for which the present theory implies an increase by a factor $(0.79)^{-3/2}$, i.e. 1.398, in the corresponding spatial growth rates $-\alpha_i^D$. This also is not inconsistent with the measured growth curves in their Figure 4. Hence as far as their Figure 4 is concerned there appears to be some agreement both on the delay of instability and on its increased growth rates, with cooling of the surface, although their interpretation (see their figures) is that the growth rates in fact decrease. The latter would seem to be due to extra normalization factors used, whereas the theory indicates that the effects of the temperature ratio T_w should be the overwhelming ones eventually, as T_w falls.

A further note of caution should be added here, concerning nonparallel-flow effects. We recall that, strictly, supersonic first modes within the wave-Mach cone are stable and governed at leading order by nonparallel-flow effects, for T_w of order unity (Smith 1987). Therefore the experimental results (of Lysenko and Maslov (1984), and others) inside the wave-Mach cone could well be influenced to a significant extent by nonparallelism rather than being true instability measurements, and they may in turn miss the new supersonic instabilities predicted for cooled surfaces.

The corresponding nonlinear processes at higher disturbance amplitudes which are noted earlier in the text should also be of much interest with respect to transition in the cooled boundary layer. For example, the nonlinear break-ups described by Smith (1988) then become attainable within finite time; and forms of vortex-wave interaction can also be induced, including those of Smith & Walton (1989) and Hall & Smith (1989). As well as the nonlinear problems mentioned in the text, that inferred from section 3(c), for reduced surface temperatures, is governed by the three-dimensional unsteady boundary-layer equations coupled with the pressure-displacement law which is given in transformed terms by (3.5b). This can be expressed as an integral relation between the unknown pressure and displacement, in two-dimensions or three-dimensions. Further, the finite time for nonlinear break-up referred to above becomes shorter as the surface is cooled, suggesting that intermittency (see references above) may arise that much sooner on a cooled surface.

There are many other regimes of concern. These include the hypersonic realm with its strong vorticity mode (Brown & Smith 1989); the transonic realm and its peculiar instability features (Bowles & Smith 1989); cross-flow effects; upper-branch properties, e.g. between the mounds of instability discussed in section 3(c); other temperature-viscosity laws, given that the Chapman assumption is vital in the new near-surface layers, although again other laws of concern seem likely to induce broadly similar behavior; and the upstream-influence analogue which is currently being considered. These additional aspects seem less significant in the long run, however, than the issues associated with nonlinearity, given the increased-instability properties found here for cooled-surface boundary layers.

Acknowledgments

References

[1] Abramowitz, M. and Stegun, I. A. (eds.), 1964, *Handbook Of Mathematical Functions*, Dover Pubs. Inc., New York.

[2] Bowles, R. I. and Smith, F. T., 1989, *On Boundary-Layer Transition In Transonic Flow*, Utd. Tech. Res. Center, East Hartford, CT, Rept. UT89.

[3] Brown, S. N. and Smith, F. T., 1989, *The Linear Inviscid Instability Of A Blasius Boundary Layer At Large Values Of The Mach Number*, submitted to J. Fluid Mech.

[4] Demetriades, A., 1978, *New Experiments On Boundary-Layer Stability Including Wall Temperature Effects*, in Proc. 1978 Heat Transfer and Fluid Mech. Inst., pp. 39-56. Stanford University Press.

[5] Gapanov, S. A. and Maslov, A. A., 1980, *Disturbance Propagation In Compressible Flows*, Nauka, Novosibirsk.

[6] Hall, P. and Smith, F. T., 1989, *Nonlinear Tollmien-Schlichting Vortex Interaction In Boundary Layers*, European J. Mechs. **B8**, 179-205 and ICASE Reports 1987-89.

[7] Kendall, J. M., 1975, *Wind-Tunnel Experiments Relating To Supersonic And Hypersonic Boundary-Layer Transition*, AIAA J. **13**, 290-299.

[8] Lin, C. C., 1955, *The Theory of Hydrodynamic Stability*, Cambridge University Press.

[9] Lysenko, V. I. and Maslov, A. A., 1981, *Transition Reversal And One Of Its Causes*, AIAA J. **19**, 705-708.

[10] Lysenko, V. I. and Maslov, A. A., 1984, *The Effect Of Cooling On Supersonic Boundary-Layer Stability*, J. Fluid Mech. **147**, 39-52.

[11] Mack, L. M., 1969, *Boundary Layer Stability Theory*, Document 900-277, Rev. A. Pasadena, Calif., JPL.

[12] Mack, L. M., 1975, *Linear Stability Theory And The Problem Of Supersonic Boundary-Layer Stability*, AIAA J. **13**, 278-289.

[13] Mack. L. M., 1984, *Boundary-Layer Linear Stability Theory*, AGARD Report 709.

[14] Mack, L. M., 1986, in *Stability Of Time Dependent And Spatially Varying Flows*, eds. D. L. Dwoyer and M. Y. Hussaini, Springer-Verlag.

[15] Malik, M. R., 1987, *Prediction And Control Of Transition In Hypersonic Boundary Layers*, AIAA paper no. 87-1414.

[16] Maslov, A. A., 1974, *The Stability Of The Supersonic Boundary Layer With Respect To A Three-Dimensional Disturbance*, Zh. Prikl. Mekh. Tekh. Fiz, 1, 37-41.

[17] Reshotko, E., 1963, *Transition Reversal And Tollmien-Schlichting Instability*, Phys. Fluids 6, 335-342.

[18] Richards, B. E. and Stollery, J. L., 1966, *Further Experiments On Transition Reversal At Hypersonic Speeds*, AIAA J. 4, 2224-2226.

[19] Smith, F. T., 1987, *On The First-Mode Instability In Subsonic, Supersonic and Hypersonic Boundary Layers*, Utd. Tech. Res. Center, East Hartford, CT, Report UT 87-52 (and 1989 J. Fluid Mech. **198**, 127-153).

[20] Smith, F. T., 1988, *Finite-Time Break-Up Can Occur In Any Unsteady Interacting Boundary Layer*, Mathematika **35**, (Part 2), 256-273.

[21] Smith, F. T., 1989, *Interactions In Boundary-Layer Transition*, in "Theor. and Applied Mechs.", ed. P. Germain, M. Piau and D. Ceillc-ie, The ier Sci. Pub., and 1989, Proc. Workshop on Boundary-Layer Instability and Transition, ICASE, May 1989, to appear in Theoretical and Computational Fluid Dynamics.

[22] Smith, F. T. and Walton, A. G., 1989, *Nonlinear Interaction Of Near-Planar TS Waves And Longitudinal Vortices In Boundary-Layer Transition*, Mathematika **36** (Part 2), to appear (see also ICASE Report 88-66).

[23] Stetson, K. F. and Rushton, G. H., 1967, *Shock Tunnel Investigation Of Boundary-Layer Transition At M=5.5*, AIAA J. 5, 899-906.

[24] Van Driest, E. R. and Blumer, C. B., 1968, *Boundary-Layer Transition At Supersonic Speeds; Roughness Effects With Heat Transfer*, AIAA J. 6, 603-607.

[25] Van Driest, E. R. and McCauley, W. D., 1957, *Boundary-Layer Transition On A 10° Cone At Mach Number 2.81 As Affected By Extreme Cooling*, J. Aeron. Sciences, October 1957, 780-781.

[26] Wisniewski, R. J. and Jack, J. R., 1960, *Recent Studies On The Effect Of Cooling On Boundary-Layer Transition At Mach 4*, J. Aeron. Sciences, March 1961, 250-251.
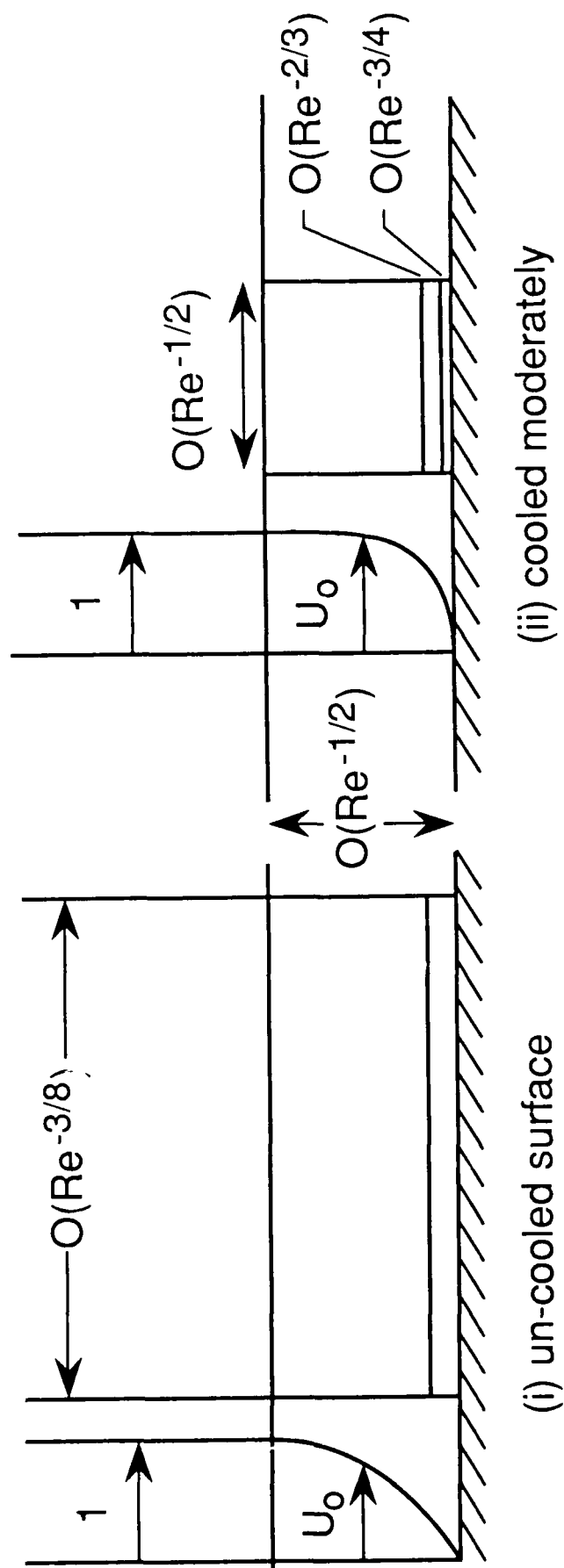
Figure 1. Effect of surface cooling on the basic compressible boundary-layer velocity profile U_0 (the temperature profile responds similarly with a large gradient at the surface), and hence on the TS instability structure for lower-branch viscous-inviscid modes studied in sections 2 and 3. The uncooled, e.g. insulated, case in (i) provokes the triple-deck structure, whereas the moderately cooled case in (ii) provokes the new structure shown, including a 2/3 buffer tier and a 3/4 viscous lower tier. Further cooling shrinks the instability structure still further, as described in sections 3(b) and 4.

Figure 2(a).
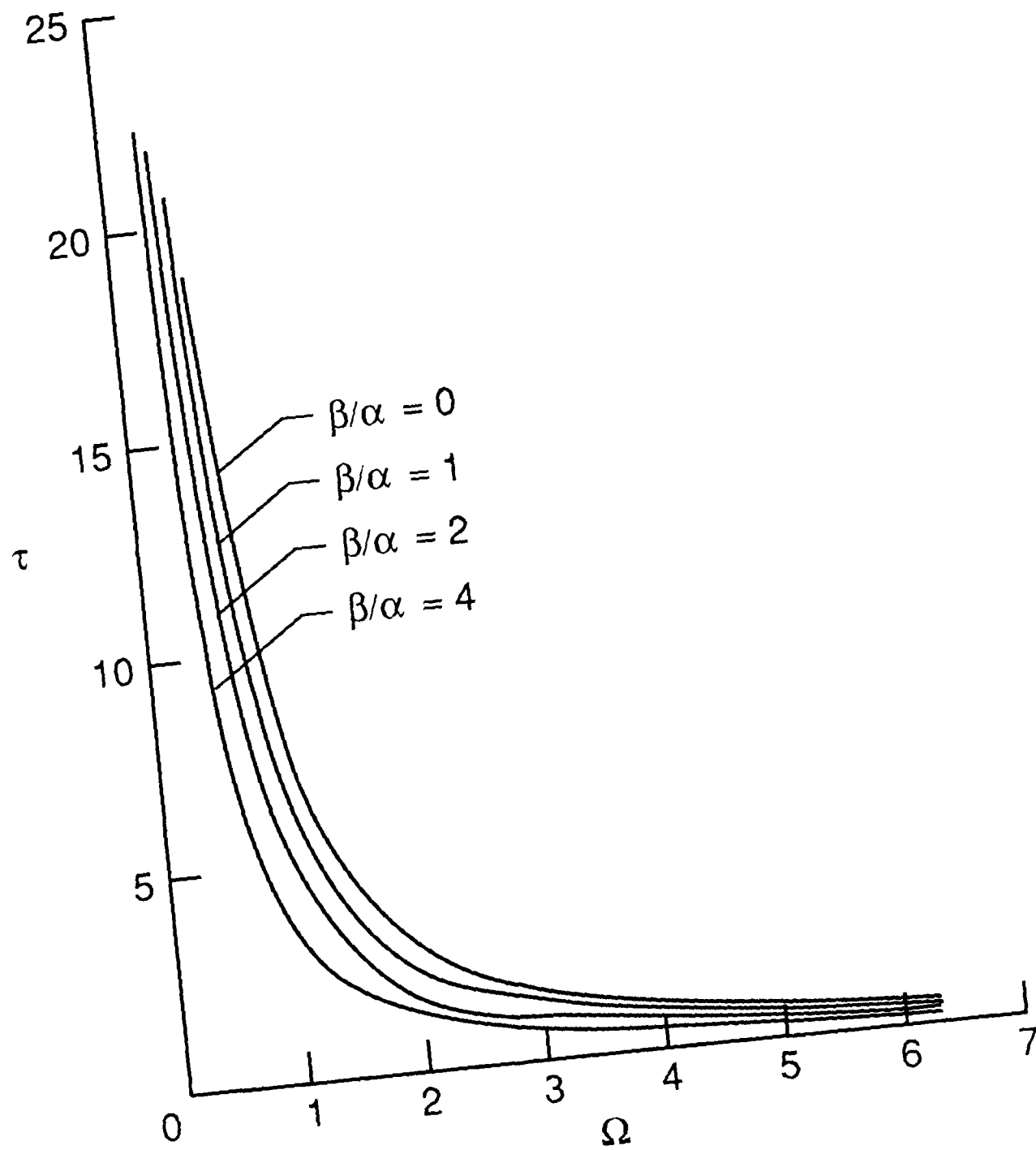
Figure 2(a). Neutral value of τ versus frequency Ω for $M_\infty = 0.5$ and $\beta/\alpha = 0, 1, 2, 4$.

Figure 2(b).
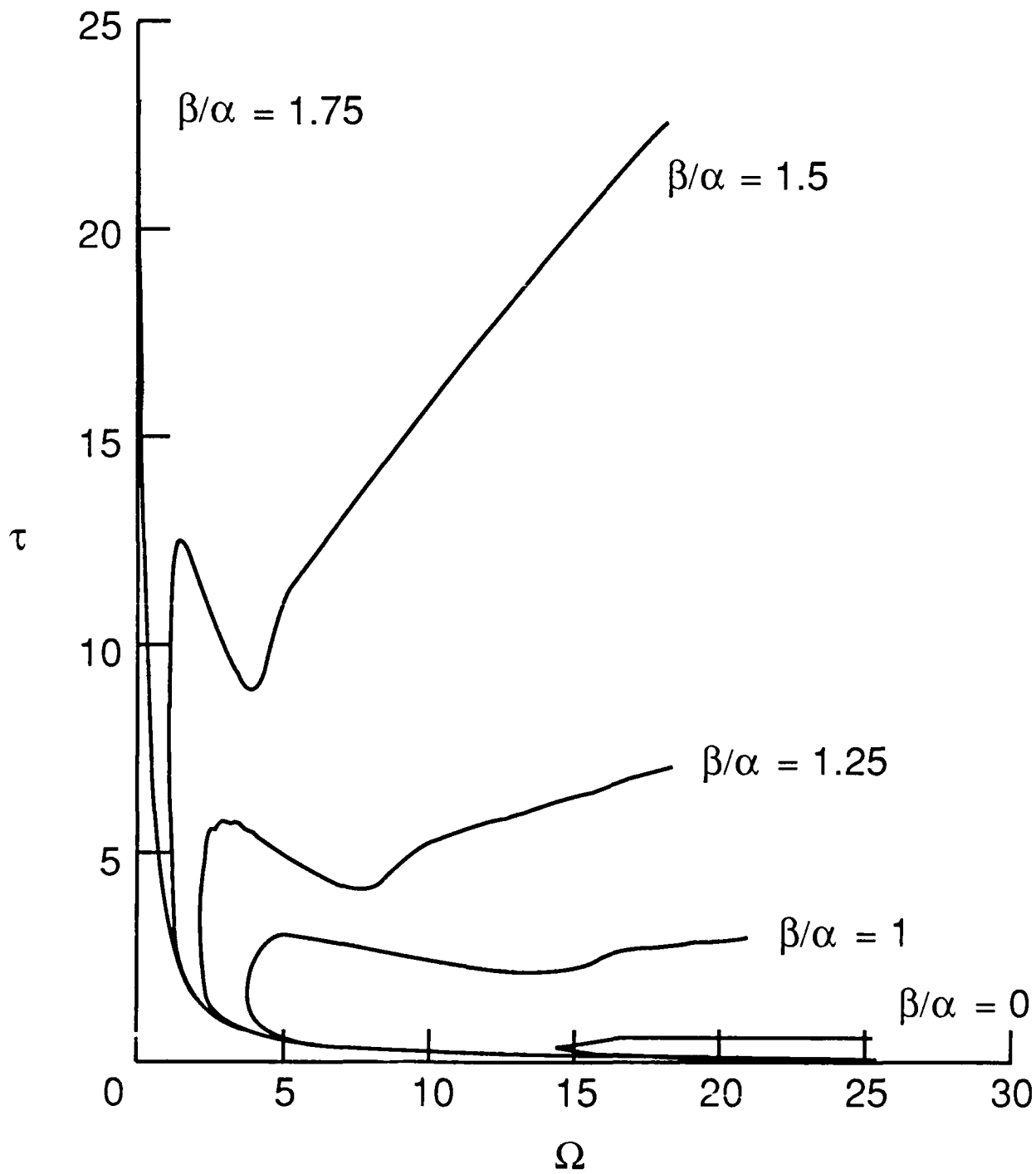
Figure 2(b). Neutral value of τ versus frequency Ω for $M_\infty = 2$ and $\beta/\alpha = 0, 1, 1.25, 1.5, 1.75$.

Figure 2(c).
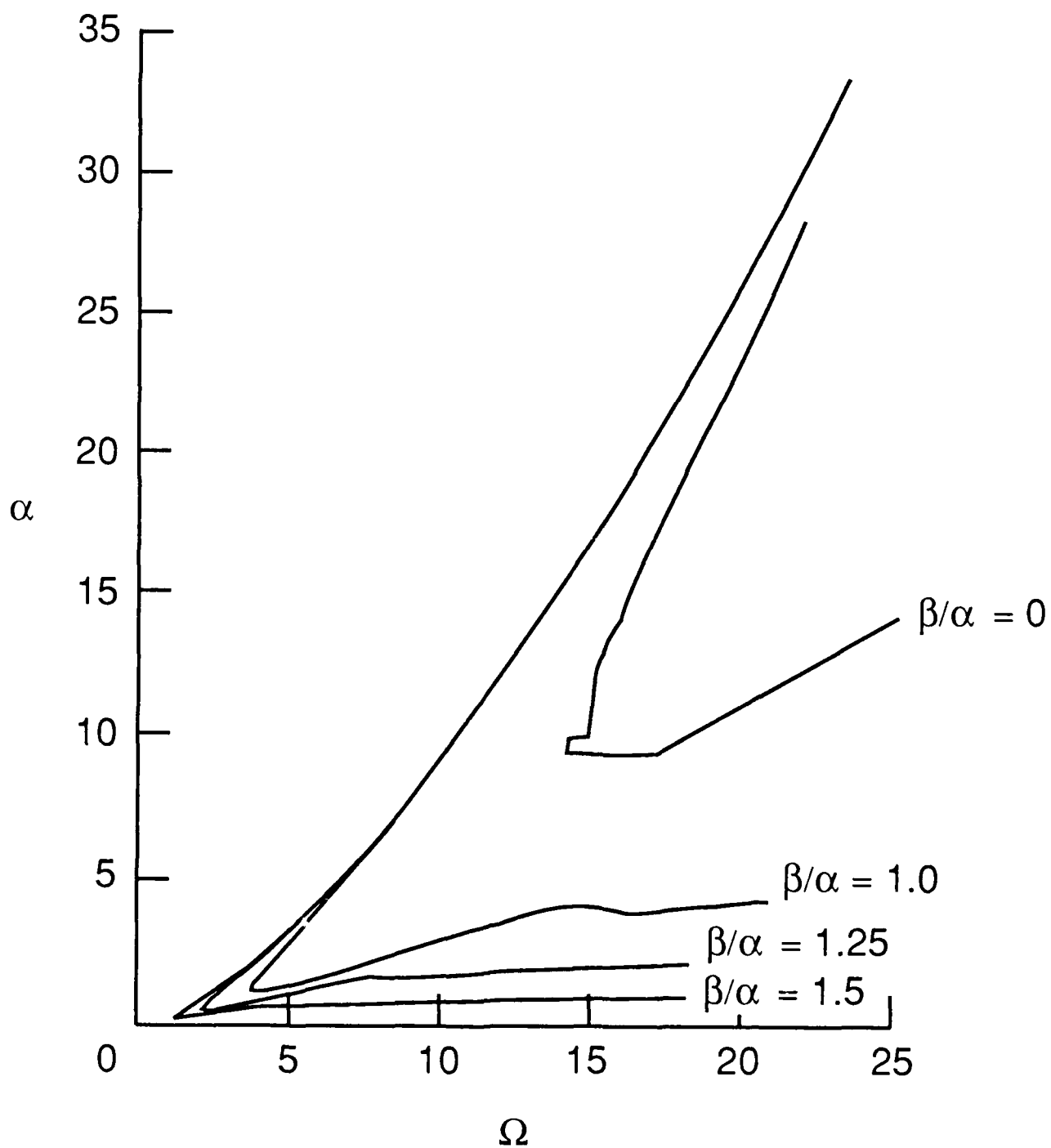
Figure 2(c). Neutral value of α versus frequency Ω for $M_\infty = 2$ and $\beta/\alpha = 0, 1, 1.25, 1.5$.

29
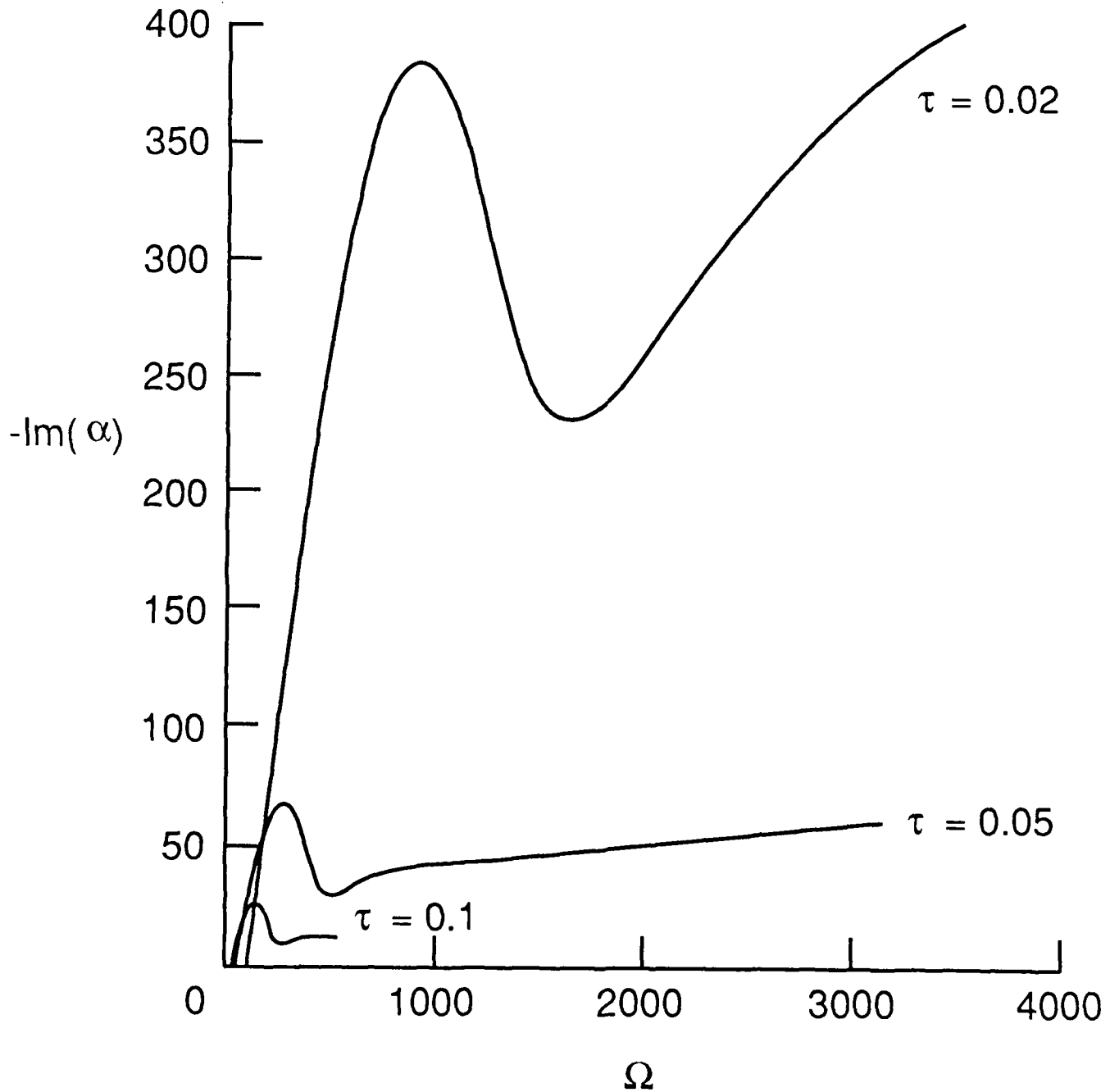
Figure 2(d).

Figure 2(d). Growth rate versus frequency Ω for $M_\infty = 0.5$, $\beta = 1$ and $\tau = 0.1, 0.05, 0.02$.

Figure 2(e).
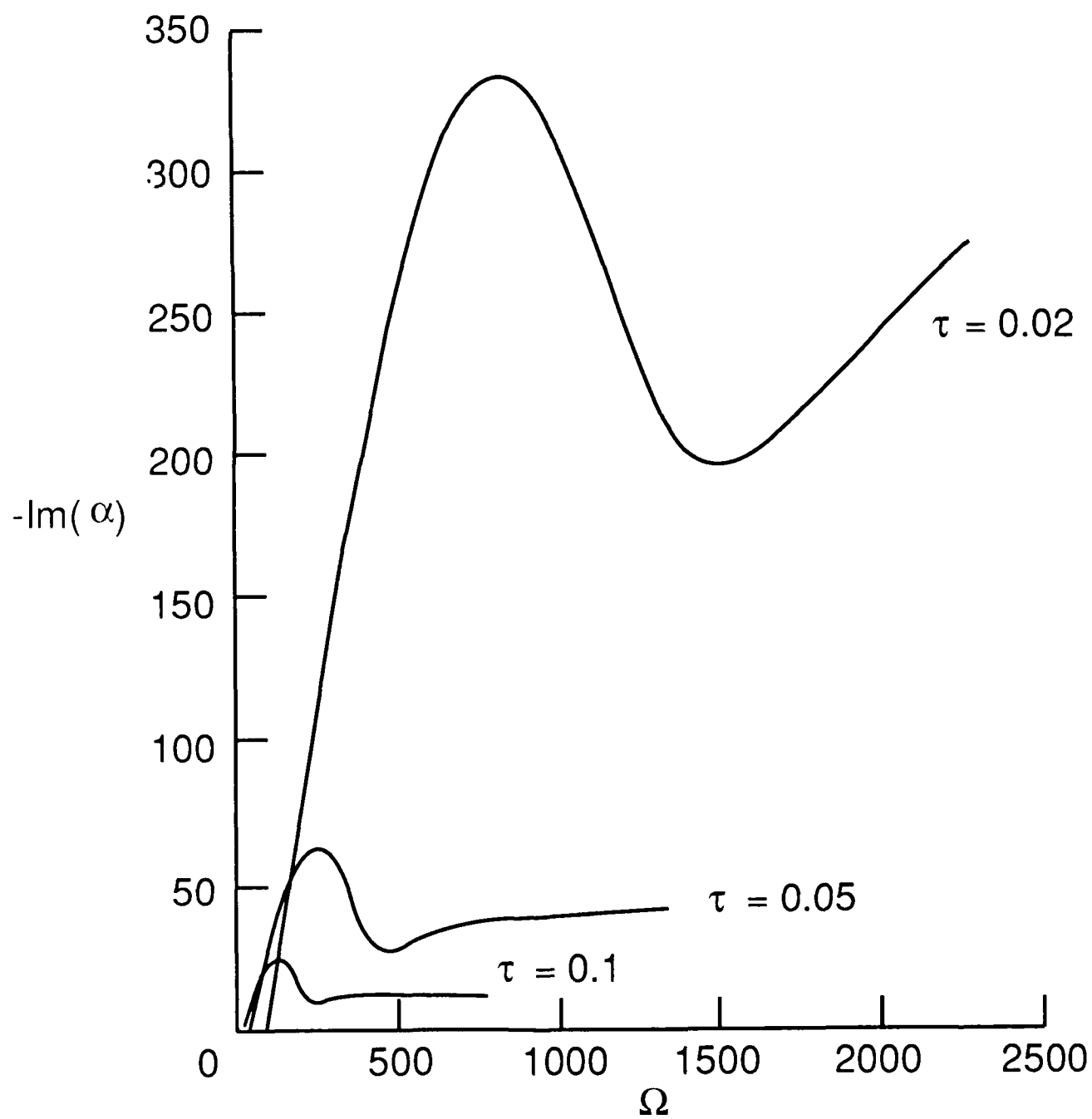
Figure 2(e). Growth rate versus frequency Ω for $M_\infty = 2$, $\beta = 1$ and $\tau = 0.1, 0.05, 0.02$.

31
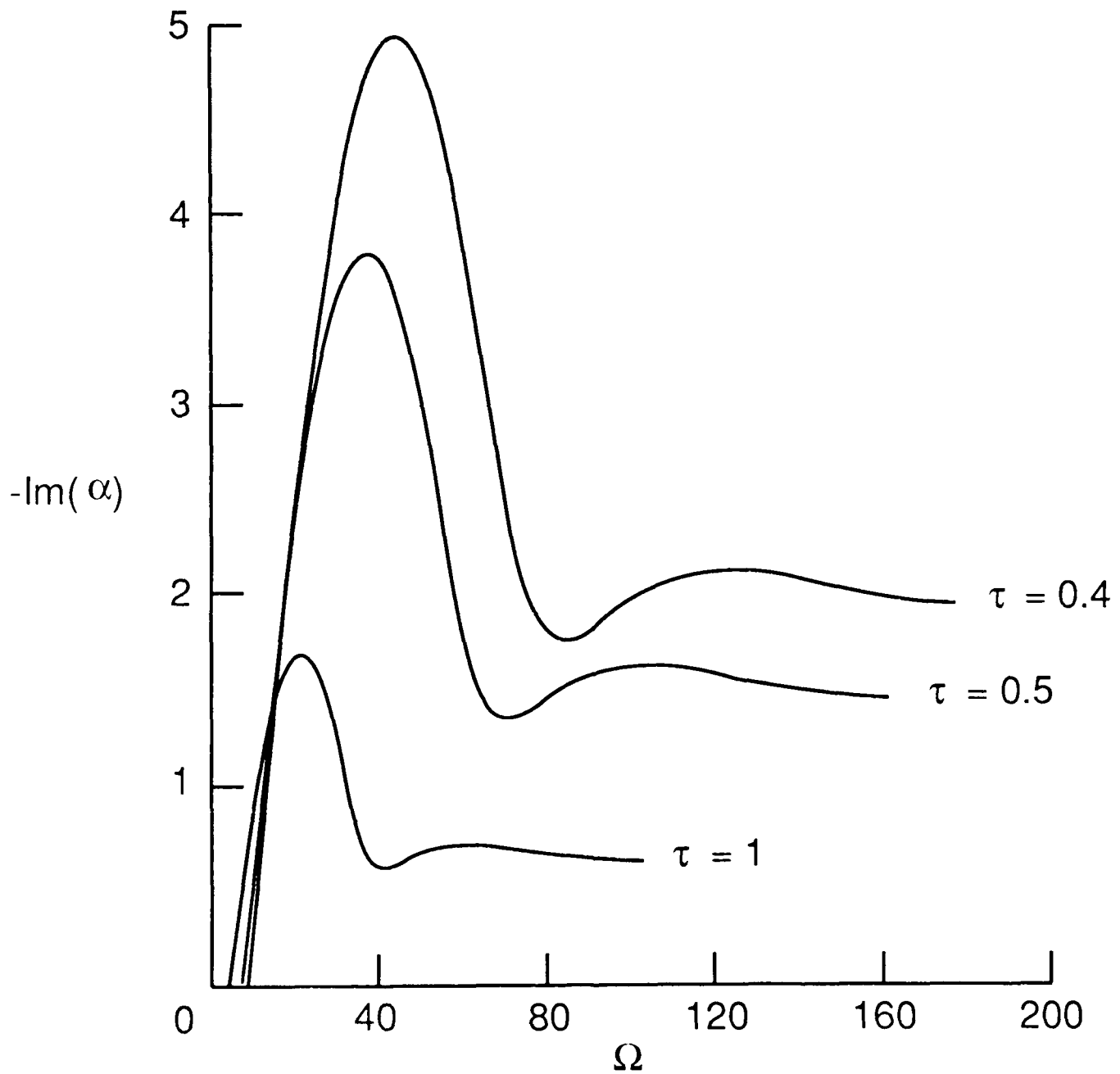
Figure 2(f).

Figure 2(f). Growth rate versus frequency Ω for $M_\infty = 0.5$, $\beta = 0$ and $\tau = 0.4, 0.5, 1$.

32
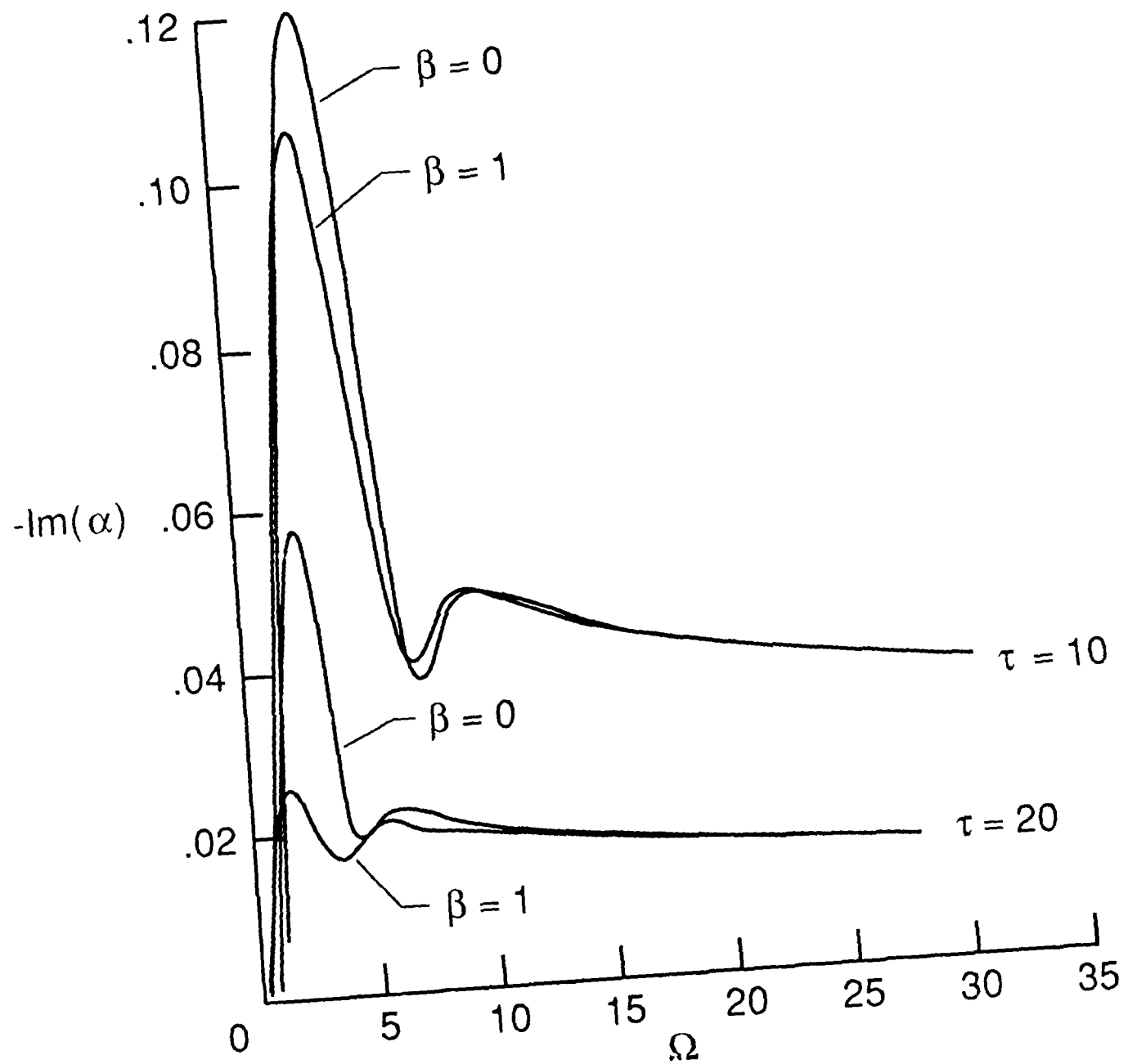
Figure 2(g).

Figure 2(g). Growth rate versus frequency Ω for $M_\infty = 0.5$, $\beta = 0, 1$ and $\tau = 10, 20$.

Figure 2(h).
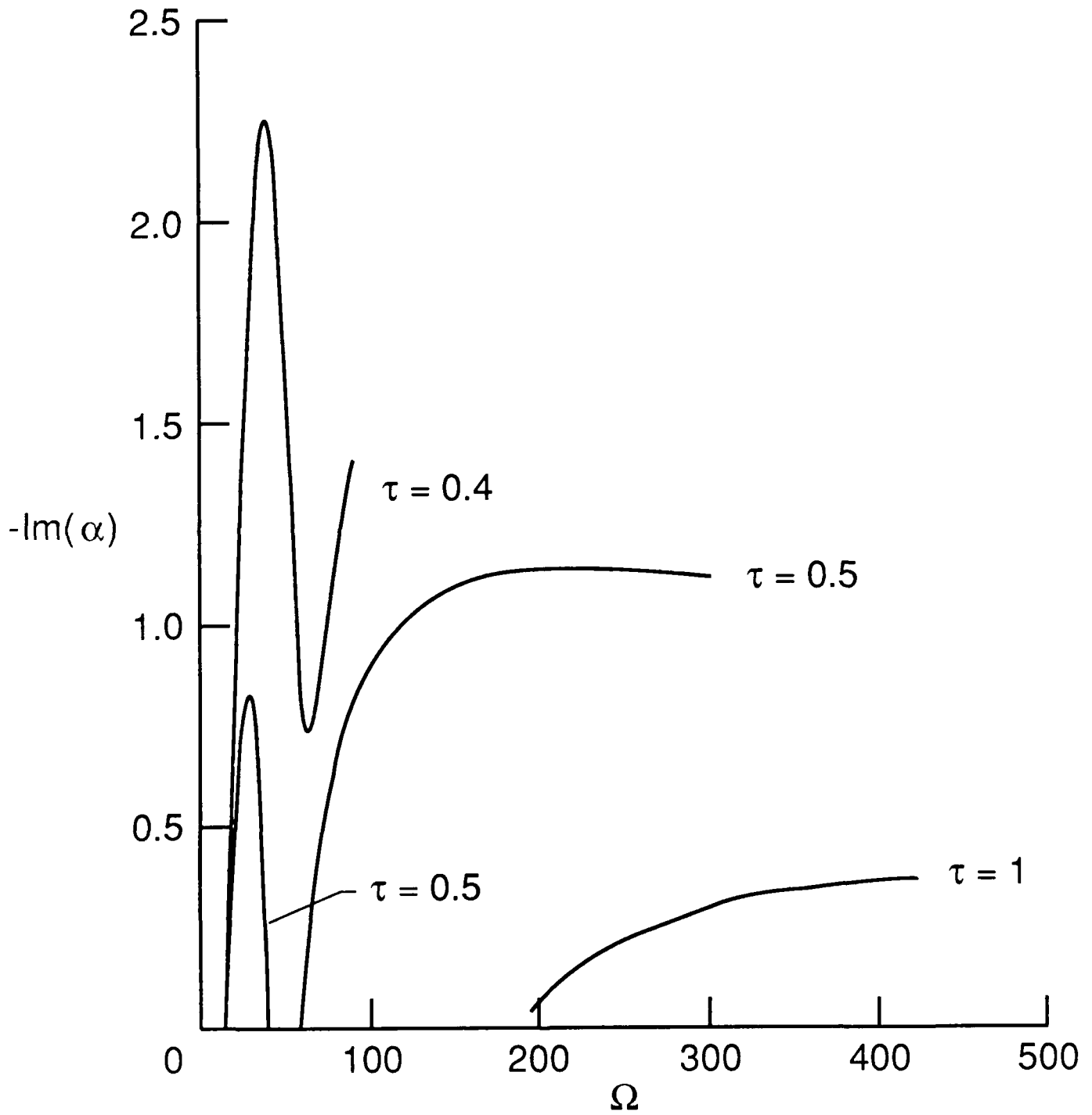
Figure 2(h). Growth rate versus frequency Ω for $M_\infty = 2$, $\beta = 0$ and $\tau = 0.4, 0.5, 1$.
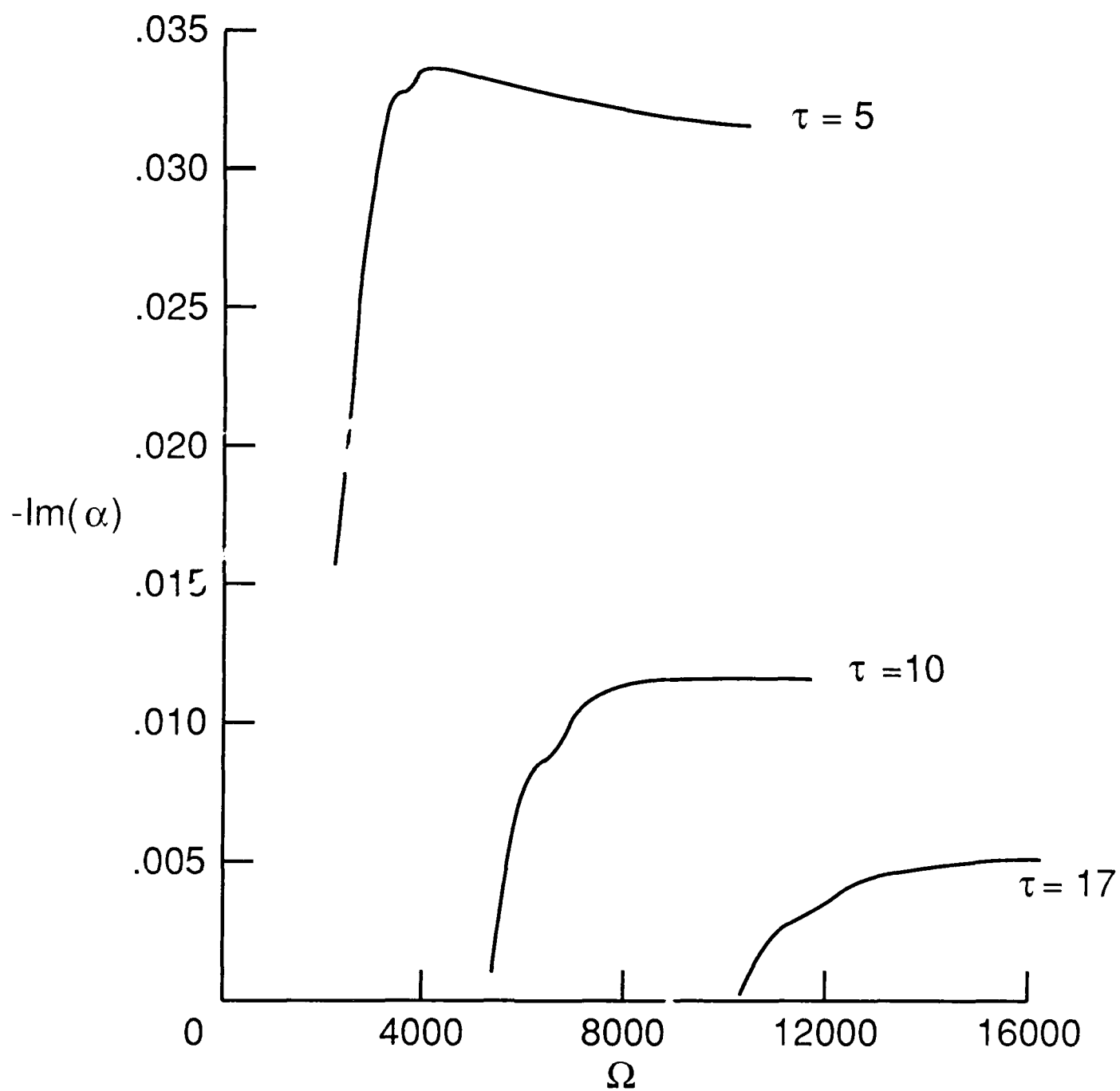
Figure 2(i). Growth rate versus frequency Ω for $M_\infty = 2$, $\beta = 0$ and $\tau = 5, 10, 17$.

35
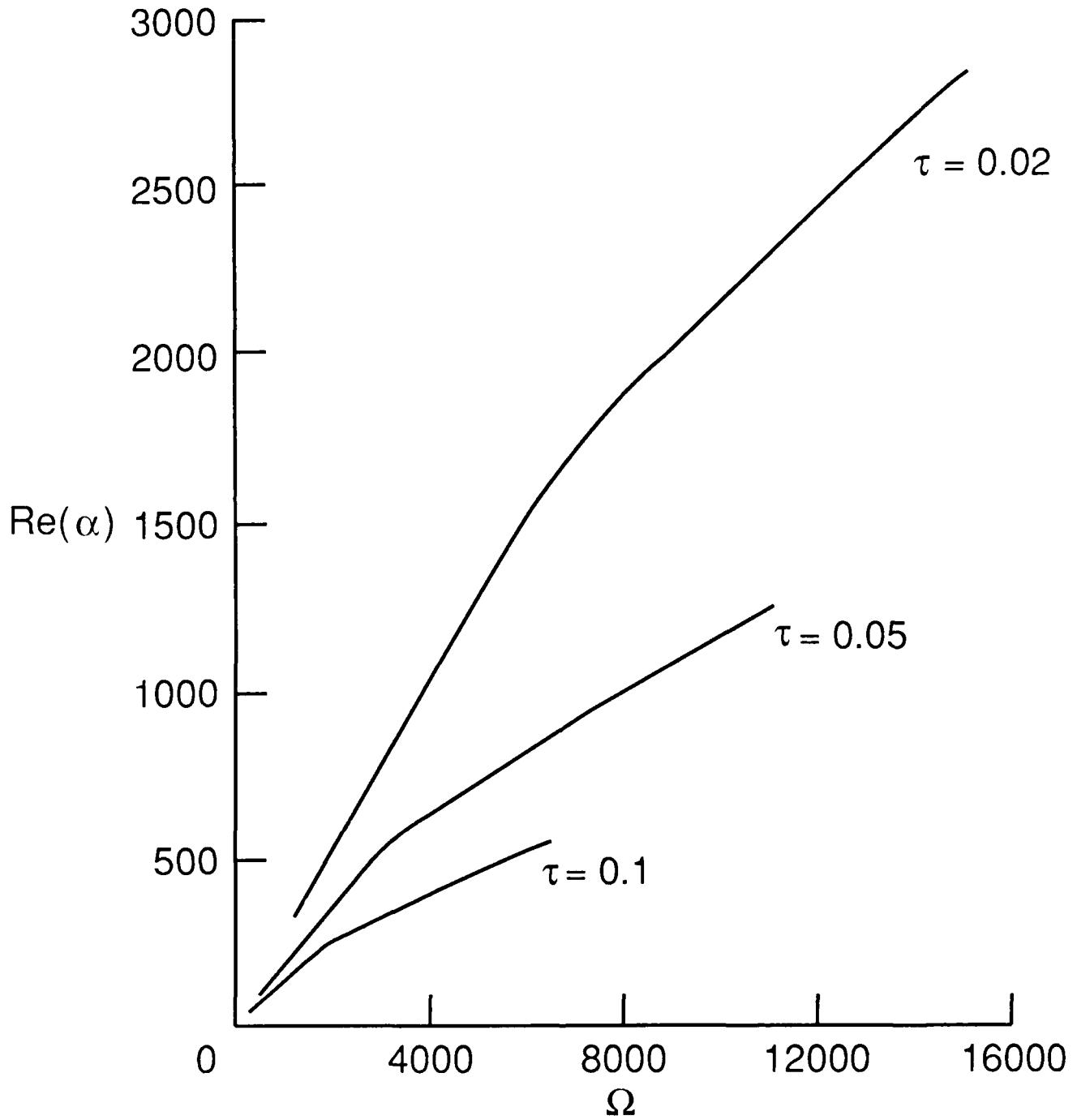
Figure 3(a).

Figure 3(a). Asymptotic solution for $Re(\alpha)$ from (3.11c) for $\tau << 1$ versus frequency Ω for $\beta = 1$ and $\tau = 0.1, 0.05, 0.02$.
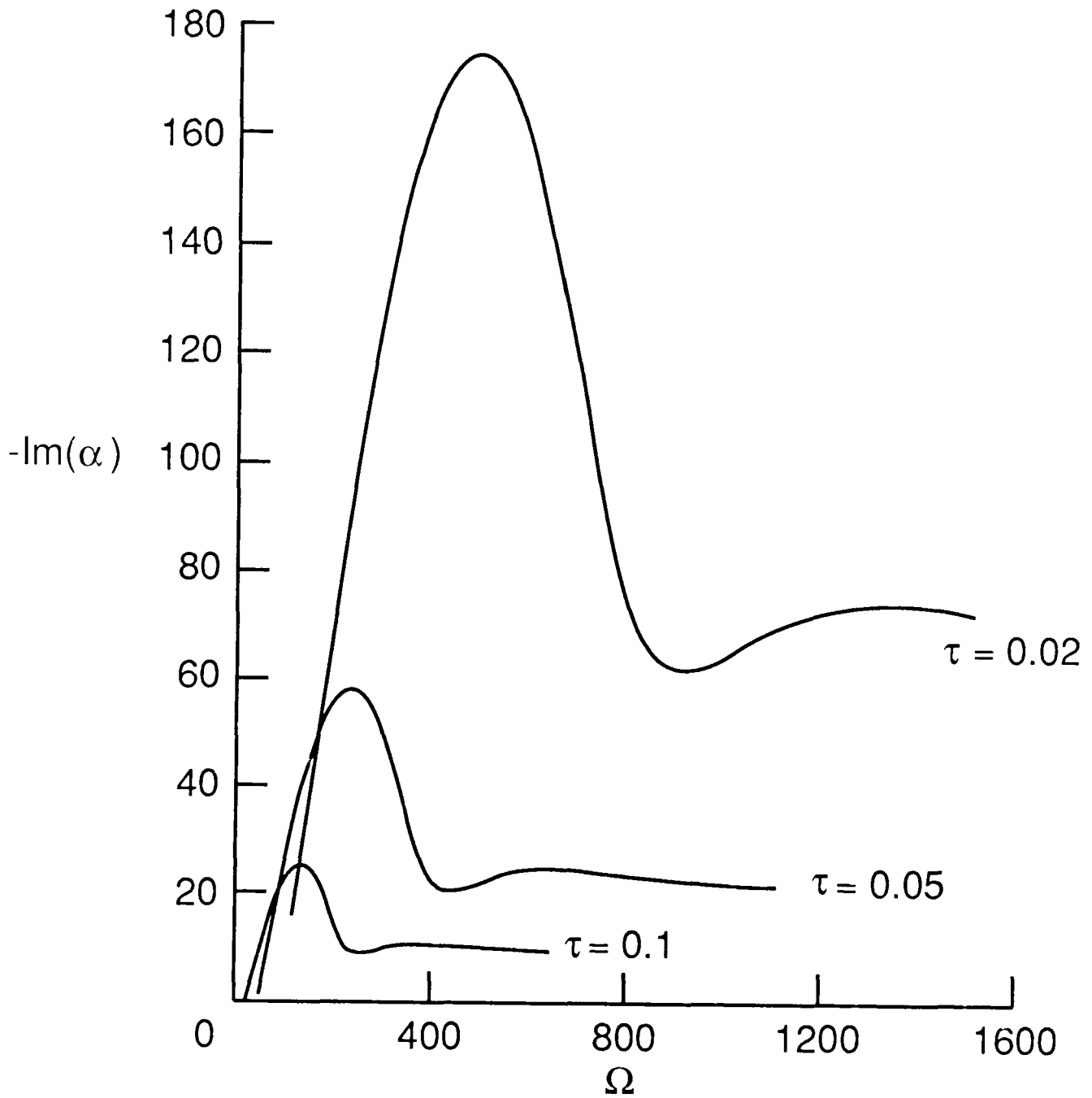
Figure 3(b). Asymptotic solution for $-Im(\alpha)$ from (3.11c) for $\tau \ll 1$ versus frequency Ω for $\beta = 1$ and $\tau = 0.1, 0.05, 0.02$.

Figure 3(c).
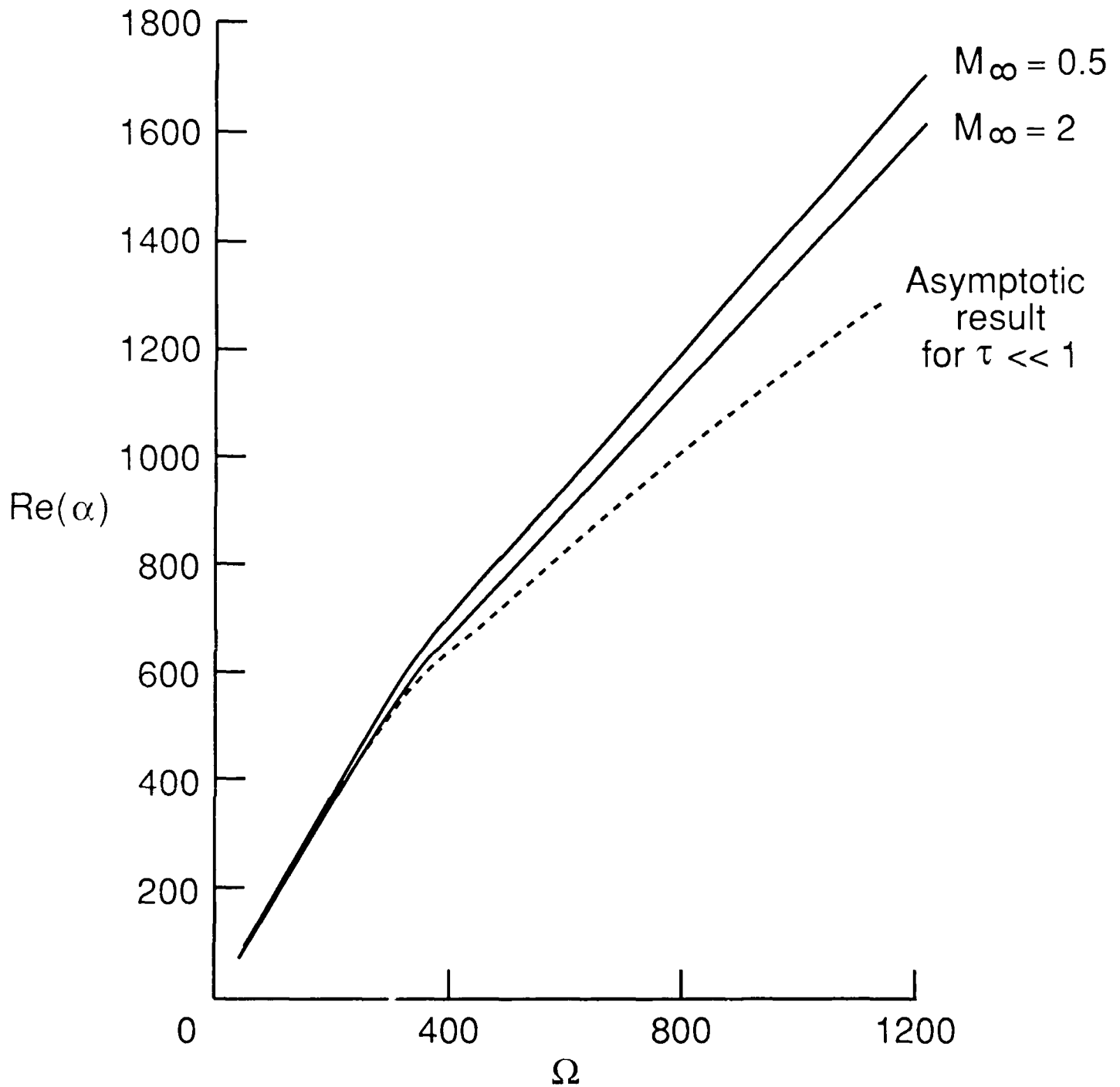
Figure 3(c). Asymptotic solution for $Re(\alpha)$ from (3.11c) for $\tau \ll 1$ versus frequency Ω for $\beta = 0$ and $\tau = 0.05$, along with the full computational solution for $M_\infty = 0.5, 2$ for comparison.

38
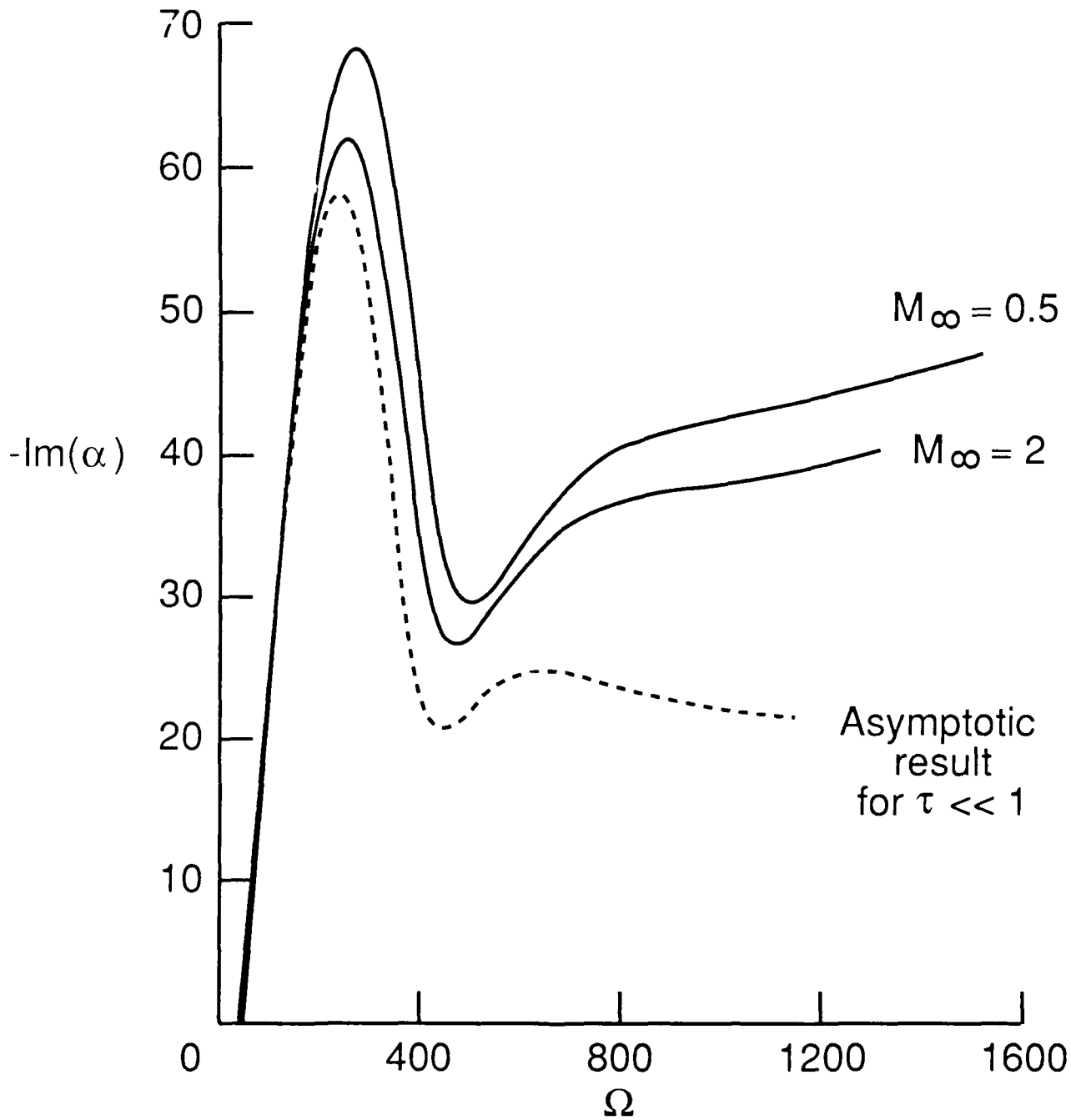
Figure 3(d).

Figure 3(d). Asymptotic solution for $-Im(\alpha)$ from (3.11c) for $\tau \ll 1$ versus frequency Ω for $\beta = 0$ and $\tau = 0.05$, along with the full computational solution for $M_\infty = 0.5, 2$ for comparison.

39
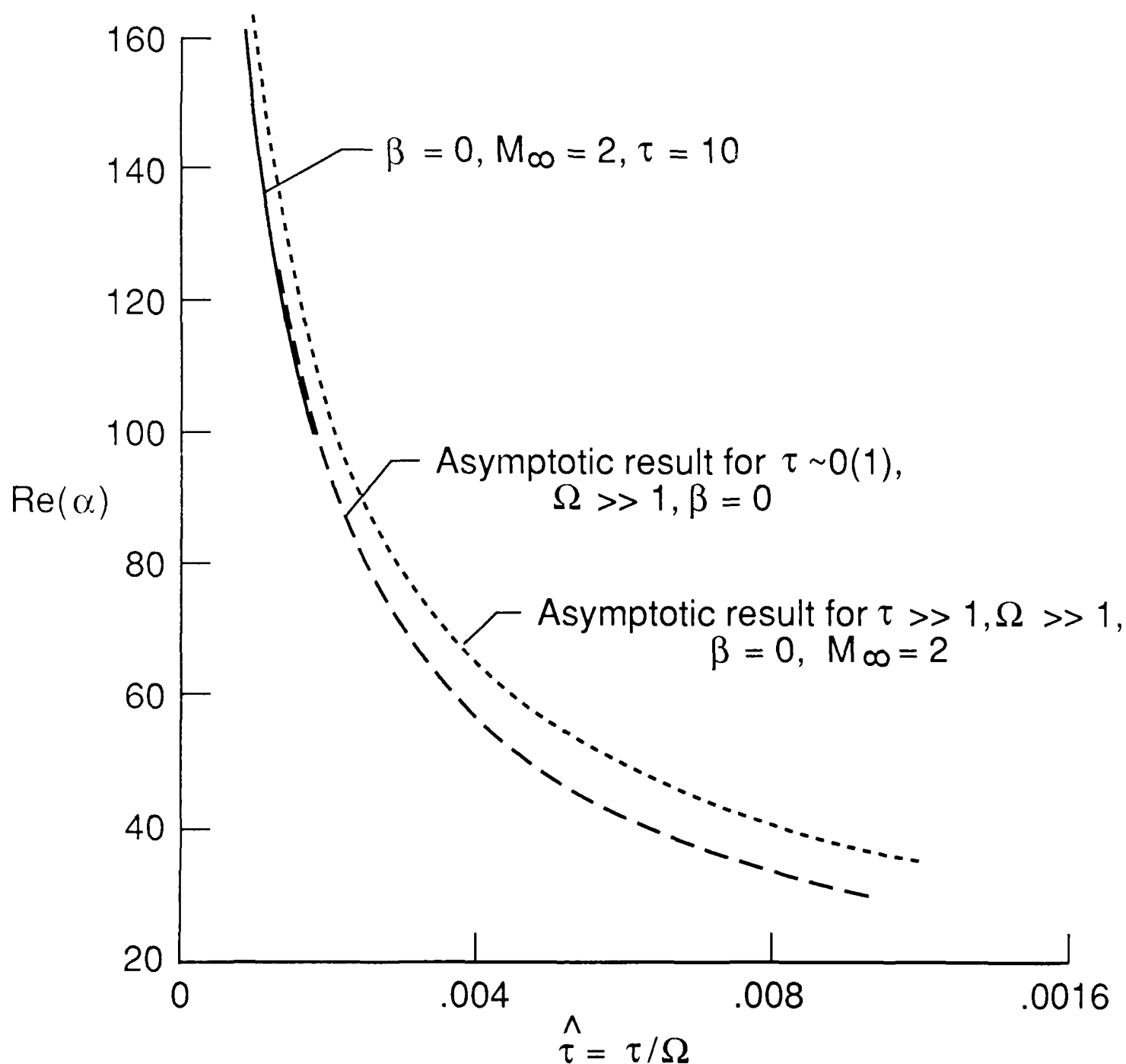
Figure 4(a).

Figure 4(a). Asymptotic solution for $Re(\alpha)$ as a function of $\hat{\tau} = \tau/\Omega$, for $\tau >> 1$ and $\Omega >> 1$ for $\beta = 0$ and $M_\infty = 2$, for $\tau \sim O(1)$, $\Omega >> 1$ and $\beta = 0$ from (3.12), along with the full computational solution for $M_\infty = 2$, $\beta = 0$ and $\tau = 10$.

Figure 4(b).
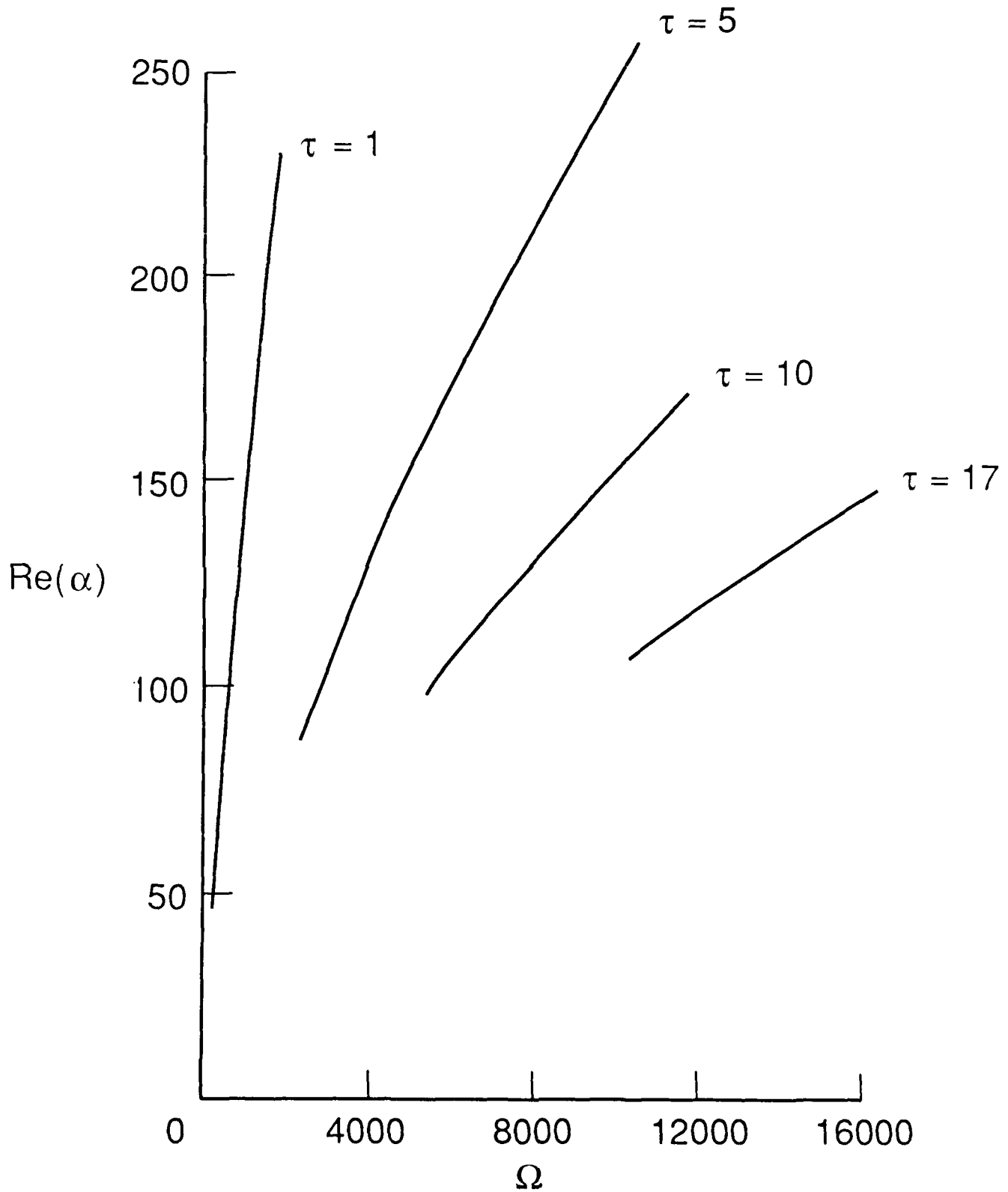
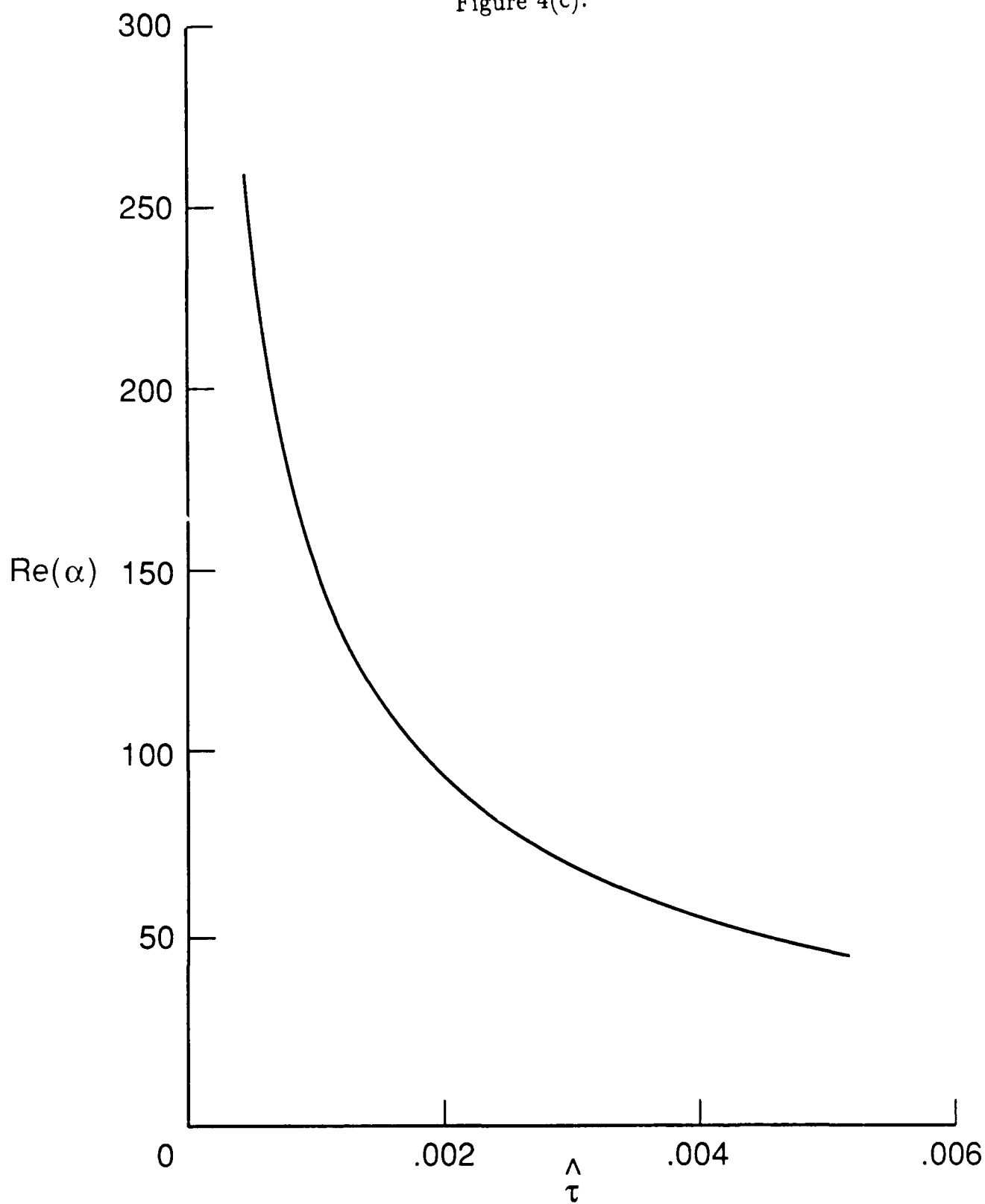Figure 4(b). $Re(\alpha)$ as a function of frequency Ω for $M_\infty = 2$, $\beta = 0$ and $\tau = 1, 5, 10, 17$.

41

Figure 4(c).

Figure 4(c). $Re(\alpha)$ as a function of $\hat{\tau}$ for $M_\infty = 2$, $\beta = 0$ and $\tau = 1, 5, 10, 17$ (curves lie on the same line).
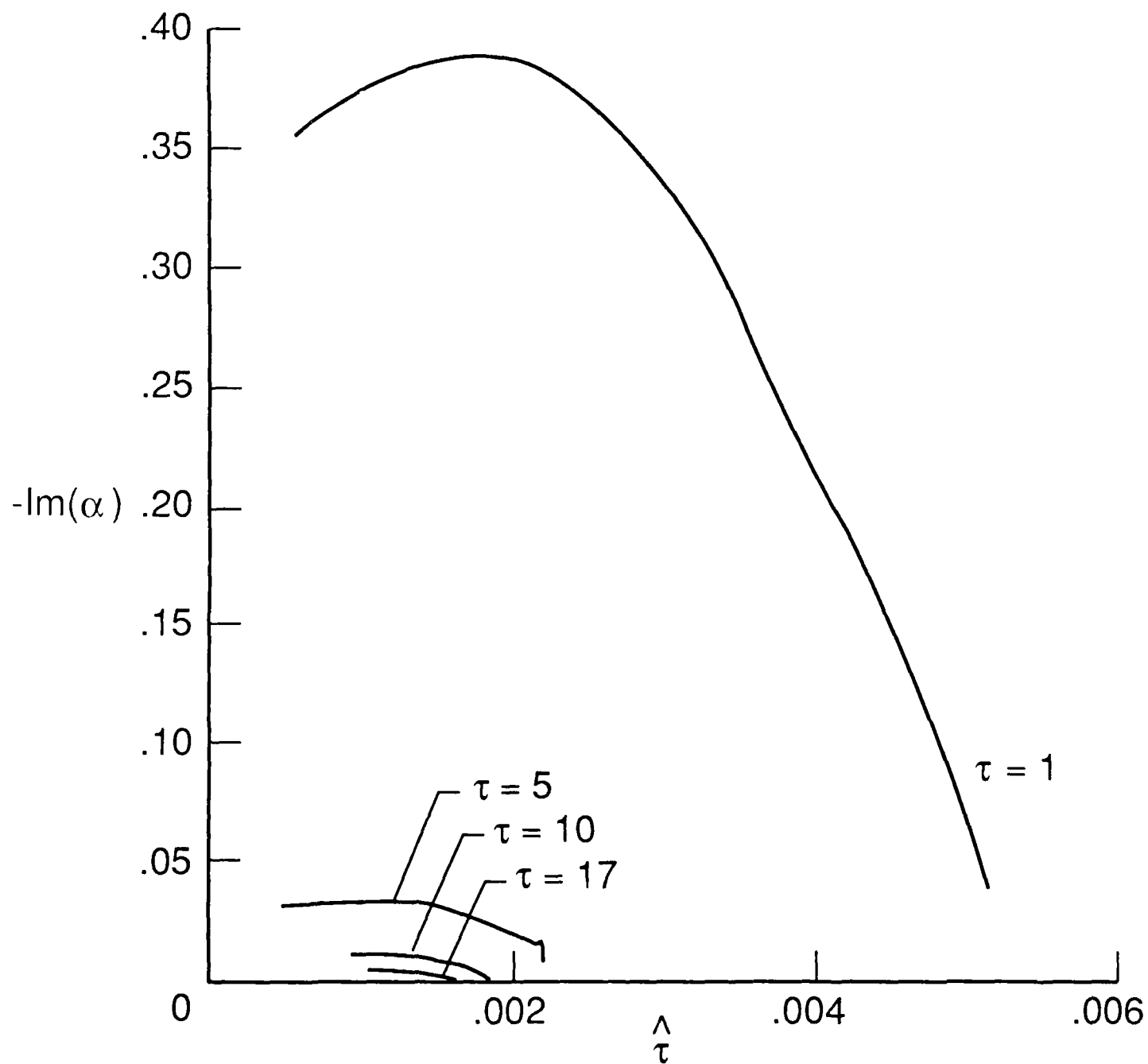
Figure 4(d).

Figure 4(d). $-Im(\alpha)$ as a function of $\hat{\tau}$ for $M_\infty = 2$, $\beta = 0$ and $\tau = 1, 5, 10, 17$.
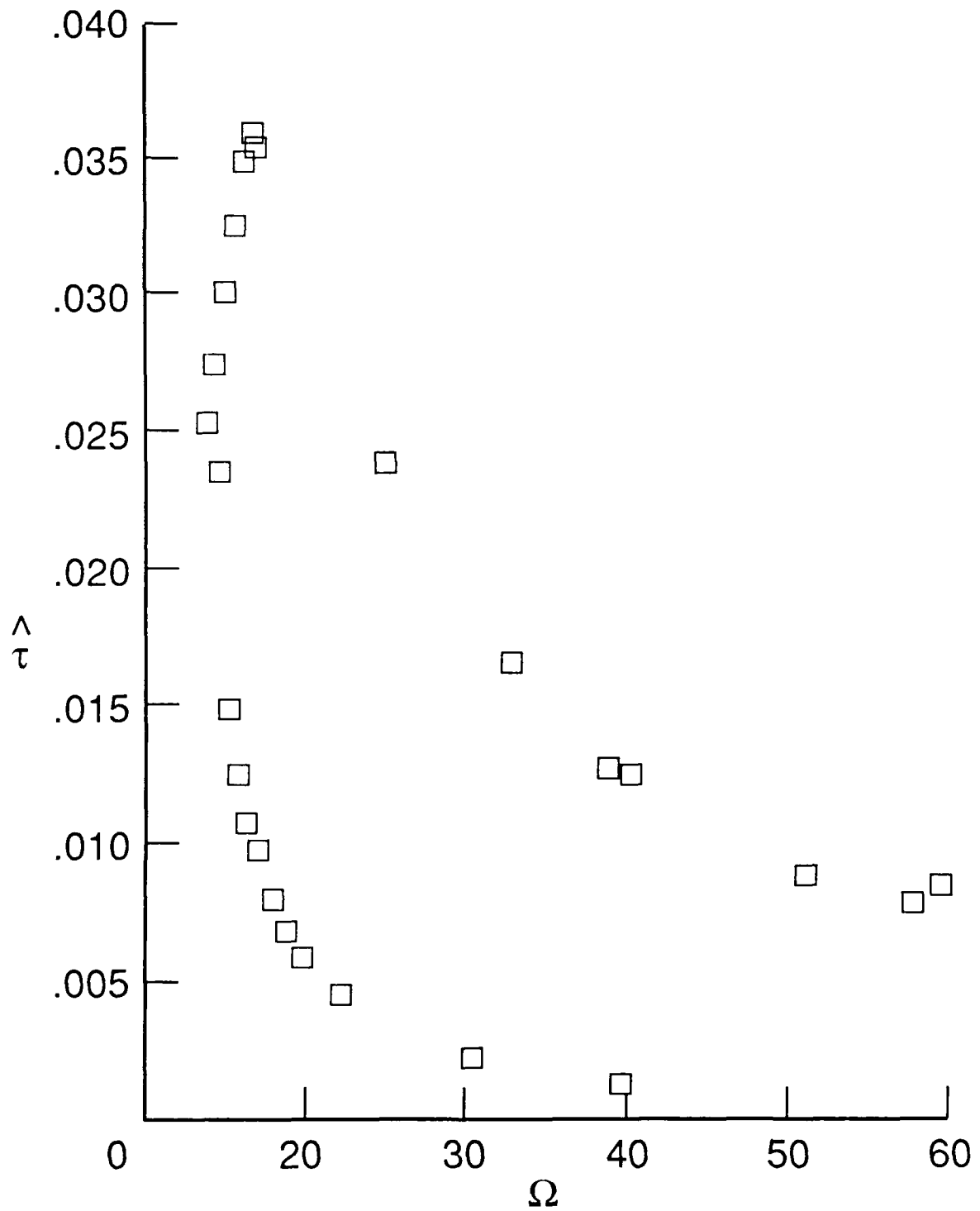
43

Figure 4(e).

Figure 4(e). Neutral value of $\hat{\tau}$ versus frequency Ω for $M_\infty = 2$ and $\beta/\alpha = 0$.
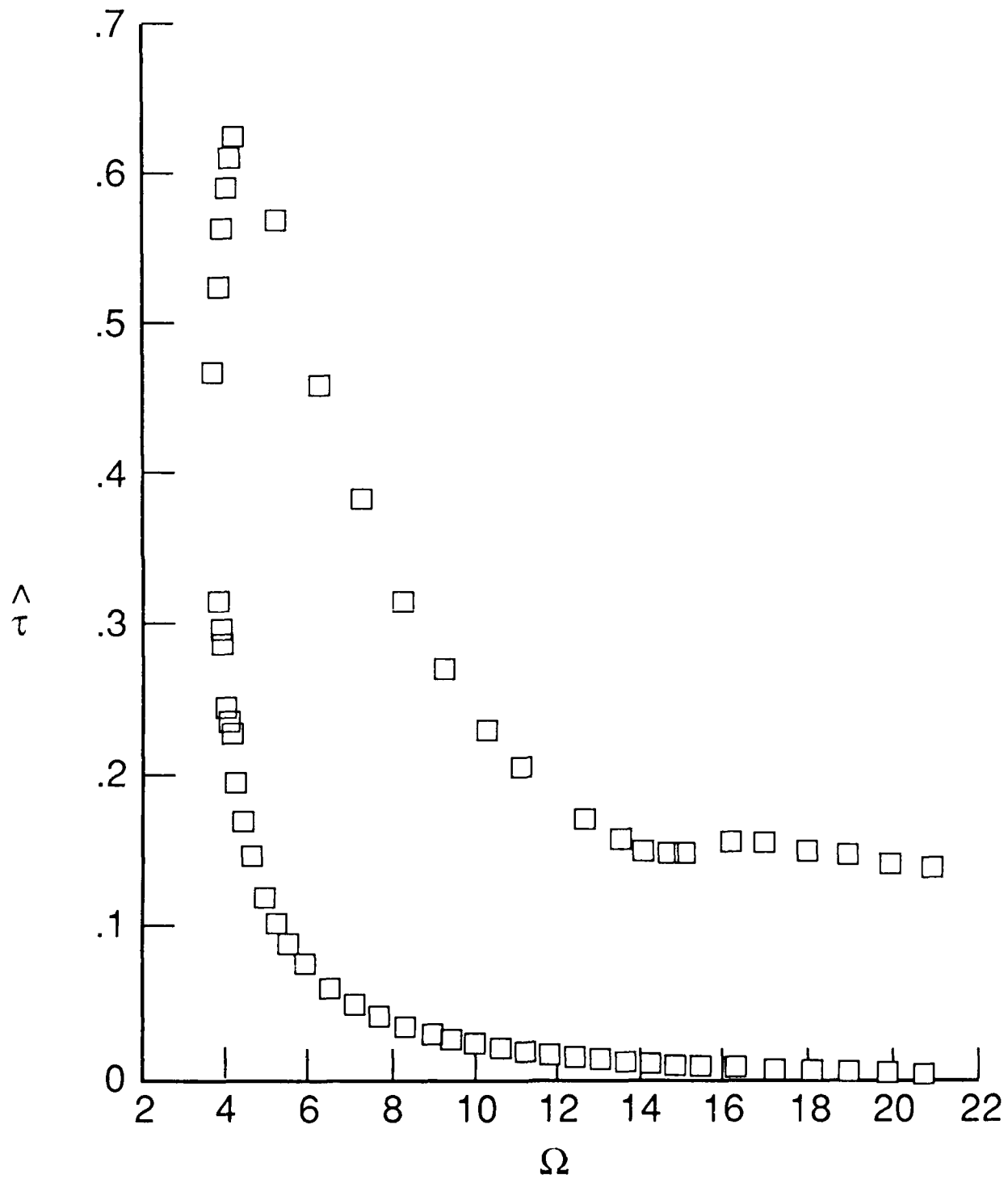
Figure 4(f).

Figure 4(f). Neutral value of $\hat{\tau}$ versus frequency Ω for $M_\infty = 2$ and $\beta/\alpha = 1$.
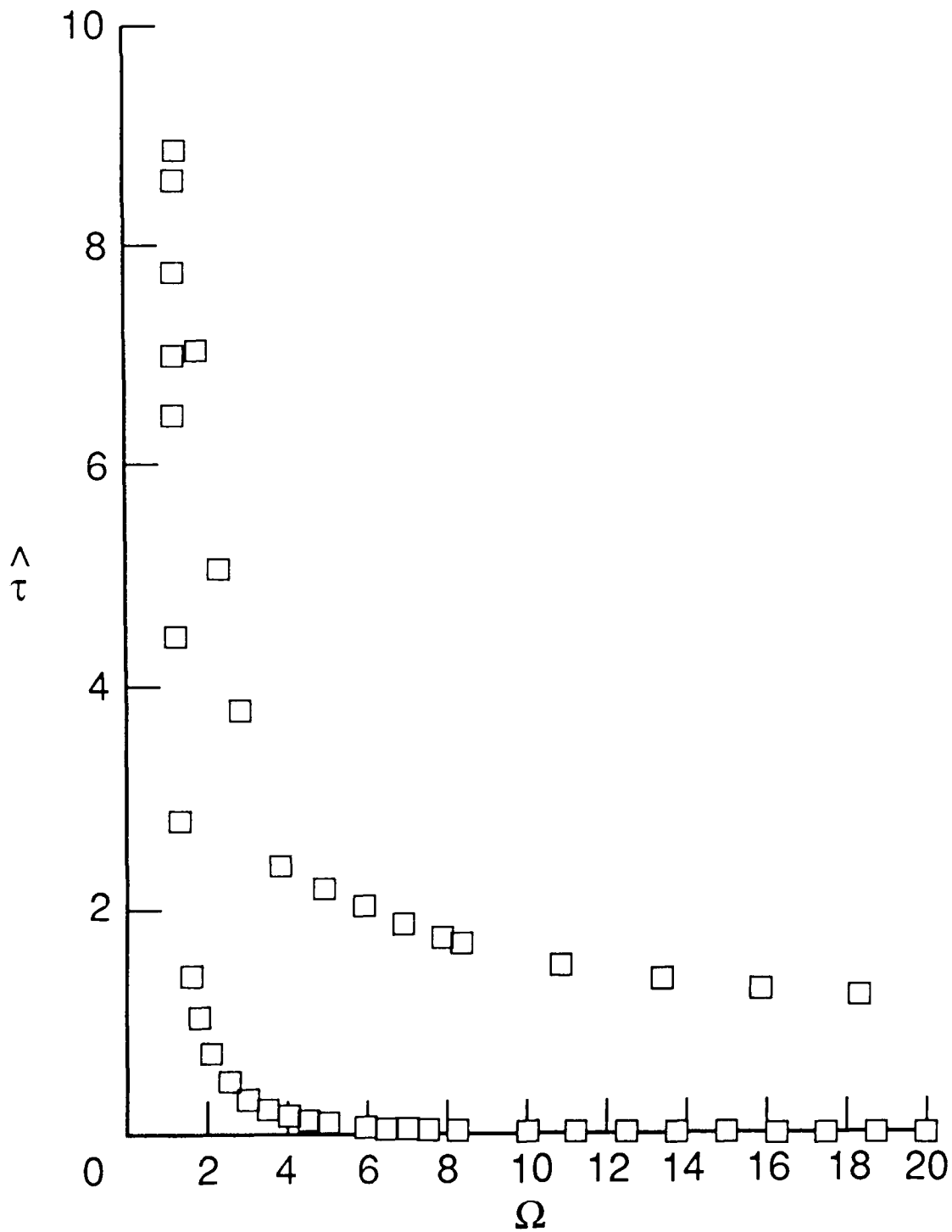
45

Figure 4(g).

Figure 4(g). Neutral value of $\hat{\tau}$ versus frequency Ω for $M_\infty = 2$ and $\beta/\alpha = 1.5$.
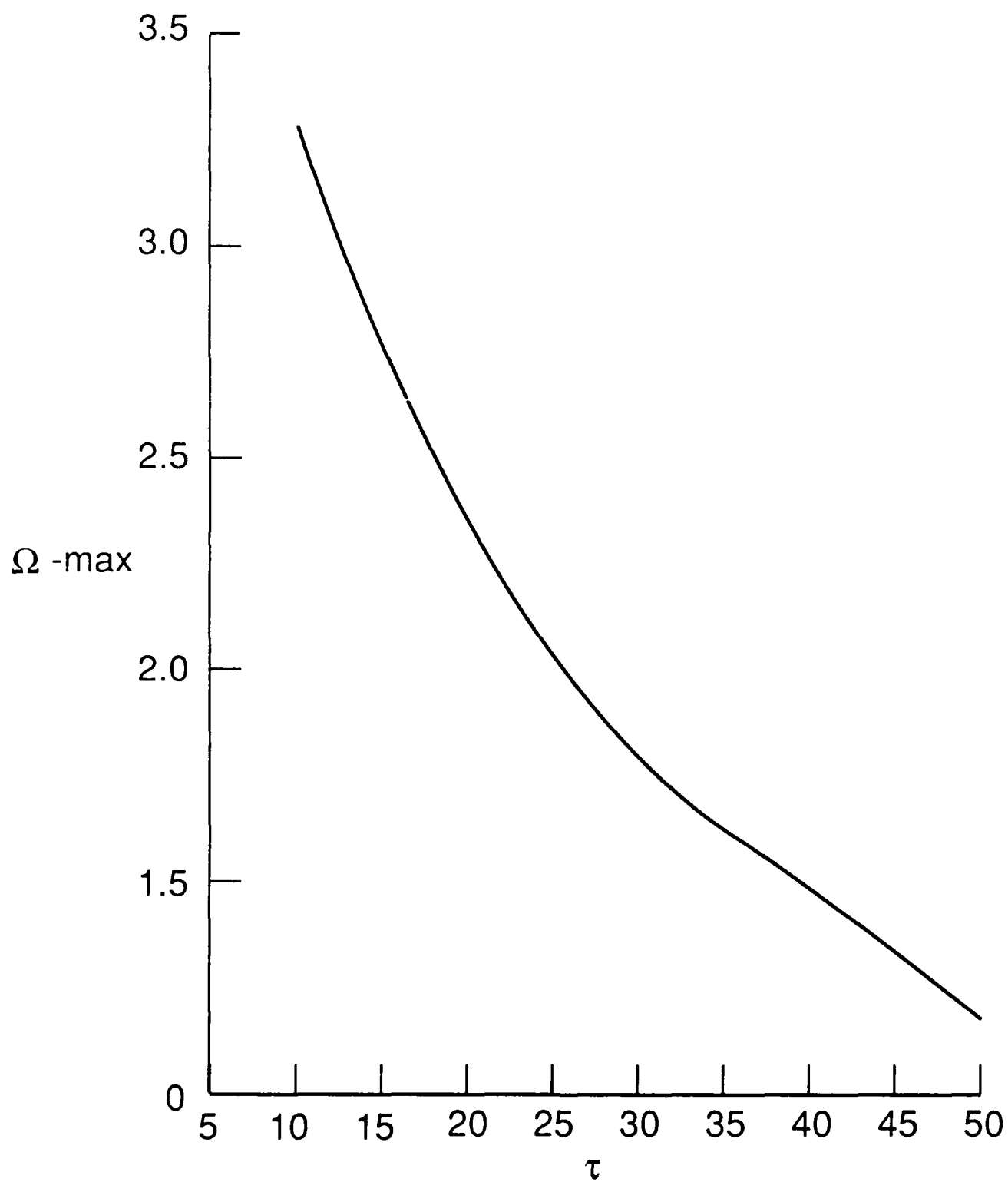
46

Figure 4(h).

Figure 4(h). $\Omega - max$ versus τ for $M_\infty = 0.5$ and $\beta = 0$
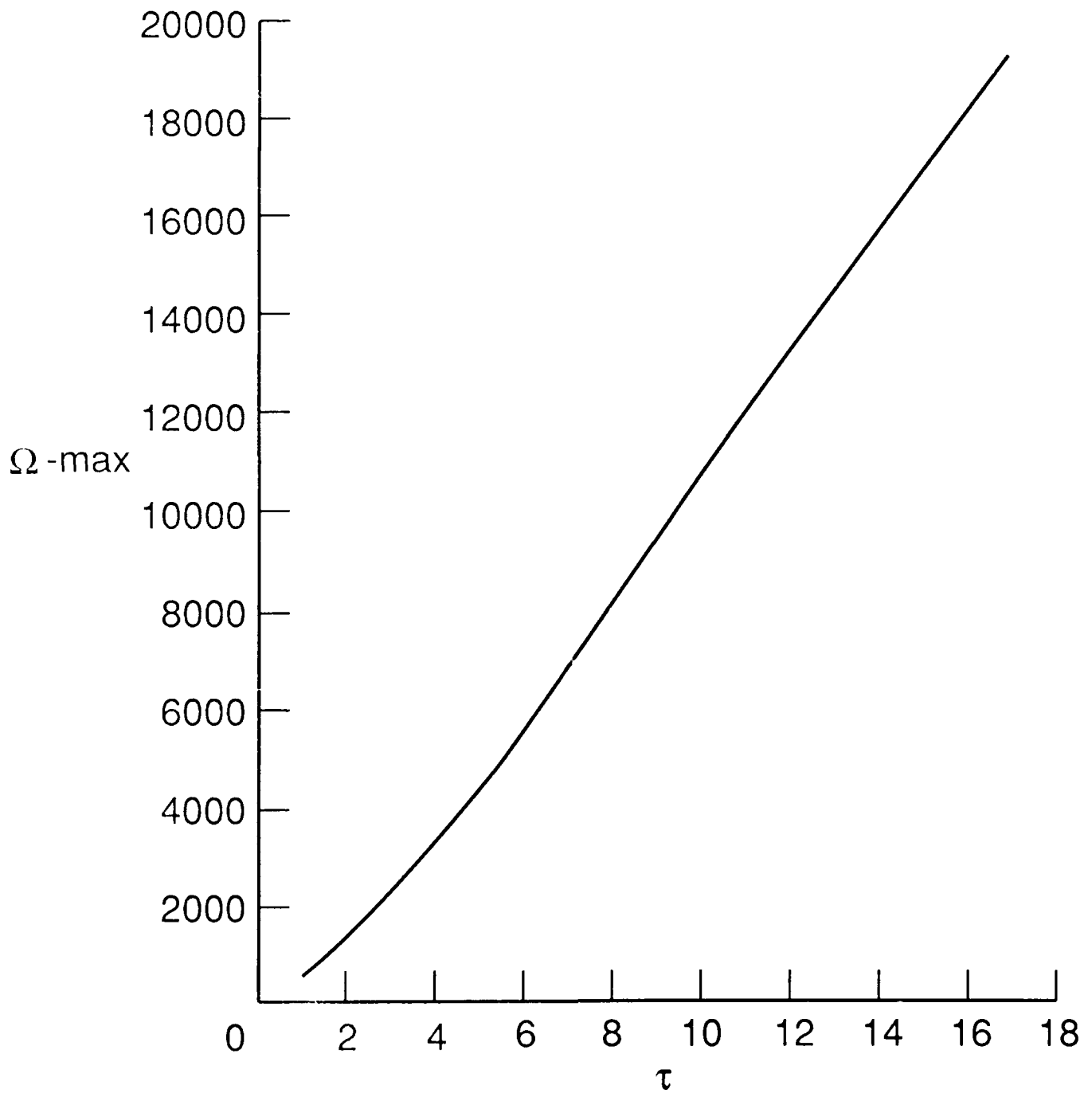
47

Figure 4(i).

Figure 4(i). $\Omega - max$ versus τ for $M_\infty = 2$ and $\beta = 0$.

48

NASA
Report Documentation Page

1. Report No. NASA CR-182003 ICASE Report No. 90-19	2. Government Accession No.	3. Recipient's Catalog No.
4. Title and Subtitle SURFACE-COOLING EFFECTS ON COMPRESSIBLE BOUNDARY-LAYER INSTABILITY		5. Report Date February 1990
		6. Performing Organization Code
7. Author(s) S. O. Seddougui R. I. Bowles F. T. Smith		8. Performing Organization Report No. 90-19
		10. Work Unit No. 505-90-21-01
9. Performing Organization Name and Address Institute for Computer Applications in Science and Engineering Mail Stop 132C, NASA Langley Research Center Hampton, VA 23665-5225		11. Contract or Grant No. NAS1-18605
		13. Type of Report and Period Covered Contractor Report
12. Sponsoring Agency Name and Address National Aeronautics and Space Administration Langley Research Center Hampton, VA 23665-5225		14. Sponsoring Agency Code

15. Supplementary Notes
Langley Technical Monitor: Richard W. Barnwell Submitted to European Journal of Mechanics Final Report

16. Abstract

The influence of surface cooling on compressible boundary-layer instability is discussed theoretically for both viscous and inviscid modes, at high Reynolds numbers. The cooling enhances the surface heat transfer and shear stress, creating a high-heat-transfer sublayer. This has the effect of distorting and accentuating the viscous Tollmien-Schlichting modes to such an extent that their spatial growth rates become comparable with, and can even exceed, the growth rates of inviscid modes, including those found previously. This is for moderate cooling, and it applies at any Mach number. In addition, the moderate cooling destabilizes otherwise stable viscous or inviscid modes, in particular triggering outward-traveling waves at the edge of the boundary layer in the supersonic regime. Severe cooling is also discussed as it brings compressible dynamics directly into play within the viscous sublayer. All the new cooled modes found involve the heat-transfer sublayer quite actively, and they are often multi-structured in form and may be distinct from those observed in previous computational and experimental investigations. The corresponding nonlinear processes are also pointed out with regard to transition in the cooled compressible boundary layer. Finally, comparisons with Lysenko and Maslov's (1984) experiments on surface cooling are presented. /

17. Key Words (Suggested by Author(s)) compressible boundary layers, instability, cooling	18. Distribution Statement 34 – Fluid Mechanics and Heat Transfer 02 – Aerodynamics Unclassified – Unlimited

19. Security Classif. (of this report) Unclassified	20. Security Classif. (of this page) Unclassified	21. No. of pages 50	22. Price A03